

Critical Exponents from AdS/CFT with Flavor

Andreas Karch,^{1*} Andy O'Bannon,^{1,2†} and Laurence G. Yaffe^{1‡}

¹*Department of Physics, University of Washington,
3910 15th Ave. NE, Seattle, WA 98195-1560, U.S.A.*

²*Max Planck Institut für Physik (Werner Heisenberg Institut)
Föhringer Ring 6, 80805 München, Germany*

ABSTRACT: We use the AdS/CFT correspondence to study the thermodynamics of massive $\mathcal{N} = 2$ supersymmetric hypermultiplet flavor fields coupled to $\mathcal{N} = 4$ supersymmetric $SU(N_c)$ Yang-Mills theory, formulated on curved four-manifolds, in the limits of large N_c and large 't Hooft coupling. The gravitational duals are probe D-branes in global thermal AdS . These D-branes may undergo a topology-changing transition in the bulk. The D-brane embeddings near the point of the topology change exhibit a scaling symmetry. The associated scaling exponents can be either real- or complex-valued. Which regime applies depends on the dimensionality of a collapsing submanifold in the critical embedding. When the scaling exponents are complex-valued, a first-order transition associated with the flavor fields appears in the dual field theory. Real scaling exponents are expected to be associated with a continuous transition in the dual field theory. For one example with real exponents, the D7-brane, we study the transition in detail. We find two field theory observables that diverge at the critical point, and we compute the associated critical exponents. We also present analytic and numerical evidence that the transition expresses itself in the meson spectrum as a non-analyticity at the critical point. We argue that the transition we study is a true phase transition only when the 't Hooft coupling is strictly infinite.

KEYWORDS: AdS/CFT, D-branes, thermal field theory.

*E-mail: karch@phys.washington.edu

†E-mail: ahob@mppmu.mpg.de

‡E-mail: yaffe@phys.washington.edu

Contents

1. Introduction	1
2. The Systems in Question	3
2.1 The Background Geometries	4
2.2 Probe Dp -branes	6
3. Scaling Analysis	11
3.1 Probe Dp -branes in $S^1 \times S^3$ Slicing: Low-temperature Phase	11
3.2 Probe Dp -branes in $S^1 \times S^3$ Slicing: High-temperature Phase	17
3.3 Probe D7-brane in Other Slicings: Low-Temperature Phase	17
4. Characterizing the Transition	19
4.1 The Behavior of $\langle \mathcal{O}_m \rangle$	19
4.2 Static Test Charges	20
4.3 The Meson Spectrum	22
4.4 Light String States	25
5. Conclusion	28

1. Introduction

The Anti-de Sitter/Conformal Field Theory (AdS/CFT) correspondence is the conjectured equivalence between $\mathcal{N} = 4$ supersymmetric $SU(N_c)$ Yang-Mills (SYM) theory and type IIB string theory formulated on the background spacetime $AdS_5 \times S^5$ [1–3]. Here, AdS_5 is a “Poincaré patch” of five-dimensional anti-de Sitter space, and S^5 is a five-sphere. The $AdS_5 \times S^5$ spacetime arises as the near-horizon geometry of $N_c \rightarrow \infty$ coincident D3-branes. Taking large N_c , small string coupling g_s , and fixed but large $g_s N_c$, the low-energy dynamics of the string theory is well-approximated by type IIB supergravity. In the SYM theory these correspond to the limits of large N_c and small g_{YM}^2 , but large ’t Hooft coupling $\lambda \equiv g_{YM}^2 N_c$.

Thermal equilibrium of the $\mathcal{N} = 4$ SYM theory corresponds to non-extremal D3-branes, whose near-horizon geometry is five-dimensional AdS-Schwarzschild times S^5 [4, 5]. The temperature of the $\mathcal{N} = 4$ SYM theory coincides with the Hawking temperature of the AdS-Schwarzschild black hole.

The $\mathcal{N} = 4$ SYM theory only contains fields in the adjoint representation of the gauge group. To make the theory more closely resemble the theory of strong interactions, Quantum Chromodynamics (QCD), we may introduce massive “flavor” fields in the fundamental

representation of the gauge group. We will introduce a finite number N_f of them, so that $N_f \ll N_c$ in the large N_c limit, and work to leading non-trivial order in N_f/N_c . These flavor fields appear in the supergravity description as N_f probe D-branes [6], or “flavor branes.” In particular, a probe D7-brane describes a massive $\mathcal{N} = 2$ supersymmetric hypermultiplet propagating in 3+1 dimensions and interacting with the $\mathcal{N} = 4$ SYM fields. In the $N_f \ll N_c$ limit, the contribution that these flavor branes make to the stress-energy tensor is dwarfed by the contribution of the N_c D3-branes. To leading order in N_f/N_c , one may neglect the back-reaction of the flavor branes on the geometry, hence the label “probe.” The flavor brane action is then the Dirac-Born-Infeld (DBI) action characterizing the embedding of the D-brane in the background spacetime.

In the supergravity description, the embedding of the D7-brane undergoes a topology-changing transition as the temperature increases. This corresponds in the dual field theory to a first-order phase transition associated with the flavor fields [7–14]. In Refs. [11, 14], analysis of a general class of probe D-brane systems (based on supersymmetry-preserving Dp - Dq intersections) revealed that in these systems the transitions associated with probe D-branes are generically first order.

In Ref. [13], two of the present authors analyzed the thermodynamics of flavor fields in the SYM theory formulated on a 3-sphere. The supergravity dual in this case does not arise as the near-horizon limit of any known D-brane construction in string theory: $\mathcal{N} = 4$ SYM formulated on a 3-sphere, in the ’t Hooft limit and at large ’t Hooft coupling, is holographically dual to supergravity formulated on *global* AdS , as opposed to Poincaré patch AdS . From the SYM theory perspective, the 3-sphere introduces a scale into the CFT allowing for a thermal phase transition. (Without such a scale to set a transition temperature, there can be no phase transition at any non-zero temperature.) At high temperature, relative to the inverse 3-sphere radius, the $\mathcal{N} = 4$ SYM theory is in a “deconfined” phase, in which the free energy scales as N_c^2 . At low temperature, however, the free energy is order one, *i.e.*, $O(N_c^0)$. A first-order phase transition separates the two phases. In the supergravity description, the transition appears as a Hawking-Page transition [4, 15] in which the high-temperature phase is global AdS -Schwarzschild and the low-temperature phase is global AdS with a periodic time direction, which we will call global thermal AdS .

We may introduce a probe D7-brane into this background, which now corresponds to adding a flavor hypermultiplet to $\mathcal{N} = 4$ SYM defined on S^3 . In the high-temperature phase, a probe D7-brane undergoes a topology-changing transition that is essentially the same as that in Poincaré patch AdS -Schwarzschild [7–14]. This, once again, represents a first-order transition in the flavor physics of the dual field theory [13]. In the low-temperature phase the probe D7-brane undergoes a different topology-changing transition. The surprising result of Ref. [13] was that this transition does not appear to correspond to a first-order transition in the SYM theory.

Our goal in this paper is to understand the nature of this transition. To do so, we will provide a more general context in which to understand the D7-brane’s transition. We will examine other probe D-branes that are supersymmetric at zero temperature (and in

the Poincaré patch), in particular a probe D5-brane [16–18], which describes flavor fields propagating in 2+1 dimensions. We will also study the $\mathcal{N}=4$ SYM theory formulated on certain other curved manifolds.

As in Refs. [11, 14, 19, 20], an essential tool in our analysis will be scaling symmetries of probe D-brane embeddings. The crucial ingredient for the arguments of Refs. [11, 14, 19, 20] was that certain scaling exponents associated with probe D-brane embedding solutions were *complex-valued*, which implied the existence of infinitely many solutions of the embedding equations (and boundary conditions). Such “multi-valued” supergravity solutions imply the presence of discontinuities in SYM theory observables. As external parameters, such as the hypermultiplet mass, are varied, the physically relevant solution can jump from one branch to another, leading to discontinuities in generic observables. (The details of the argument will be reviewed below.)

We will find that the D7-brane in global thermal AdS has *real-valued* exponents, and that this will lead to very different physical consequences. Our general analysis will reveal the condition that determines whether the scaling exponents are complex or real. In the D-brane’s topology change, we can identify a “critical solution” intermediate between the two topologies. The dimension of the submanifold that collapses to zero volume in this critical solution determines whether the scaling exponents will be real or complex.

For the D7-brane in global thermal AdS we will further characterize the transition by computing two observables that are especially convenient to evaluate using the supergravity description: the expectation value of the hypermultiplet mass operator (*i.e.*, the supersymmetric completion of $\bar{\psi}\psi$), and the expectation value of a particular supersymmetric Polyakov loop correlator. We will find that both have derivatives that diverge near the critical point, and we will compute the associated critical exponents. We will also compute the meson spectrum of the SYM theory from fluctuations of the D7-brane’s worldvolume fields. We will find that the transition appears in the meson spectrum as a non-analyticity, a cusp, in the spectrum of one scalar meson. Lastly, we will argue that the transition is only a genuine phase transition in the flavor physics at infinite ’t Hooft coupling, that is, the divergences we find in derivatives of the free energy only exist when λ is strictly infinite.

This paper is organized as follows. In section 2 we present in greater detail the systems that we will study. In section 3, we perform the scaling analysis, compute the scaling exponents, and present numerical evidence that complex exponents signal a first-order transition in the SYM theory. In section 4, we compute the critical exponents and meson spectrum for the SYM theory dual to the probe D7-brane in global thermal AdS , and argue that the transition will be smoothed out at finite λ . We conclude with a brief discussion in section 5.

2. The Systems in Question

We begin with a more precise description of the supergravity systems we will study. After reviewing global AdS and introducing our conventions, we describe the relevant probe D-brane embeddings in greater detail.

2.1 The Background Geometries

We are interested in $\mathcal{N} = 4$ SYM theory formulated on curved spatial sections. We work in the limits of large N_c and large 't Hooft coupling, $\lambda \equiv g_{YM}^2 N_c \gg 1$ so that, via the AdS/CFT correspondence, we may compute observables in the SYM theory using supergravity. We are thus interested in global AdS_5 , whose boundary is a curved four-manifold. Global AdS_5 does not arise from any known string theory construction (such as a near-horizon geometry of very many D-branes), so we must assume that the conjectured equivalence of theories, originally motivated by the black D3-brane solution of type IIB string theory [1], can be extended to include supergravity on global AdS_5 .

As we will be studying the thermodynamics of the SYM theory, we introduce a temperature T in the standard fashion by working in Euclidean signature and compactifying the time direction into a circle of radius $R_1 = 1/(2\pi T)$. We will mainly be interested in the SYM theory formulated on a spatial 3-sphere (times time). We denote the radius of the 3-sphere as R_3 . We will thus be studying the SYM theory formulated on boundary spacetimes such as $S^1 \times S^3$.

We will use a global thermal AdS_5 metric

$$ds^2 = d\rho^2 + \cosh^2 \rho d\tau^2 + \sinh^2 \rho d\Omega_3^2, \quad (2.1)$$

where we have set the curvature radius of AdS_5 equal to one. We will work in these units throughout. In these units, we convert between string theory and SYM quantities using the relation $\alpha'^{-2} = 4\pi g_s N_c = g_{YM}^2 N_c = \lambda$, where α' is the square of the string length: $\alpha' \equiv \ell_s^2$. In Eq. (2.1), ρ is the radial coordinate, τ is the compact Euclidean time coordinate of period $1/T$, and $d\Omega_3^2$ is the metric of a unit 3-sphere. The center of the AdS space is at $\rho = 0$, and the boundary is at $\rho = \infty$. Notice in particular that the 3-sphere collapses to zero volume at the center of AdS .

We will also frequently find another coordinate system convenient, a so-called Fefferman-Graham coordinate system [21] in which the radial coordinate is $z = e^{-\rho}$, so that the center of AdS_5 is at $z = 1$ and the boundary is at $z = 0$. The global AdS_5 -Schwarzschild metric, written in this Fefferman-Graham coordinate system, is

$$ds^2 = \frac{1}{z^2} [dz^2 + g_{ij} dx^i dx^j], \quad (2.2a)$$

with

$$g_{ij} dx^i dx^j \equiv \frac{1}{4} (1 - z^4/z_H^4)^2 \mathcal{F}(z)^{-1} d\tau^2 + \frac{1}{4} \mathcal{F}(z) d\Omega_3^2, \quad (2.2b)$$

$$\mathcal{F}(z) = 1 - 2z^2 + z^4/z_H^4, \quad (2.2c)$$

and $z_H \equiv [1 + 4(\pi T)^4]^{-1/4}$ is the horizon radius. Setting $z_H = 1$ produces the global thermal AdS_5 metric, Eq. (2.1), in Fefferman-Graham coordinates. Notice that in our units the radius of the 3-sphere at the boundary is $R_3 = 1/2$.

When discussing global thermal AdS_5 , we will use the ρ coordinate unless stated otherwise. When discussing AdS_5 -Schwarzschild, we will use only the z coordinate.

A Hawking-Page transition [15] connects global thermal AdS_5 and global AdS_5 -Schwarzschild. This is a first order transition associated with black hole condensation. The two metrics written above are both solutions to Einstein's equation with constant negative curvature and an asymptotic boundary that is $S^1 \times S^3$. The difference of the Einstein-Hilbert action for these two solutions may be interpreted as a difference in free energies (divided by the temperature), and thus determines which geometry is thermodynamically preferred. Thermal AdS_5 is preferred (has lower free energy) at low temperatures, but a first-order transition occurs at a non-zero critical temperature $T_{HP} = \frac{3}{2\pi}$ (in units of the AdS radius), above which AdS_5 -Schwarzschild is preferred [4, 15]. This is a topology-changing transition: the topology of thermal AdS_5 is $\mathbb{R}^4 \times S^1$ while that of AdS_5 -Schwarzschild is $\mathbb{R}^2 \times S^3$ [4, 15].

This transition is interpreted in the boundary SYM theory as a deconfinement transition [4]. As the SYM theory is in finite volume, we must be careful to define what we mean by the word ‘‘confinement.’’ A sufficient definition for our purposes may be given in terms of the large- N_c behavior of the free energy: if the order N_c^2 contribution to the free energy is zero, we declare the theory to be in a confined phase, whereas if the order N_c^2 contribution is nonzero we declare the theory to be in a deconfined phase. In this sense, the $\mathcal{N} = 4$ theory on $S^1 \times S^3$ is in a confined phase at low temperature and in a deconfined phase at high temperature, with a first-order transition separating the two phases. In the absence of fundamental representation matter fields, this criterion is equivalent to defining a deconfined phase as one in which the \mathbb{Z}_{N_c} center symmetry is spontaneously broken in the $N_c \rightarrow \infty$ limit, which is possible even in finite spatial volume.

Notice also that the only scales in the SYM theory are the temperature T and the radius of the 3-sphere R_3 , and hence the only physically meaningful quantity is the dimensionless product TR_3 . We may interpret the limit $TR_3 \rightarrow \infty$ either as a high-temperature limit in fixed volume or as a large-volume limit at fixed temperature. We will be working in a fixed volume, so we will interpret this as a high-temperature limit. In this limit our analysis should agree with any known physics of the finite-temperature SYM theory in flat space. From the supergravity perspective, our analysis should agree with any known physics in Poincaré-patch AdS_5 -Schwarzschild.

In the course of our analysis we will study the SYM theory formulated on other curved manifolds besides $S^1 \times S^3$. To do so, we will exploit the fact that global AdS admits various ‘‘ slicings.’’ To understand these, recall that at the boundary of AdS space the metric has a second-order pole. To extract a boundary metric from a bulk AdS metric, we must choose a defining function which is arbitrary save for one feature: it has a second-order zero at the boundary. Multiplying the bulk metric by this defining function will produce a finite boundary metric. Different slicings of AdS are simply coordinate reparameterizations that naturally suggest different defining functions. Implicitly, we will be using these ‘‘natural’’ defining functions, which give rise to boundaries with different geometries. We will be interested in

slicings producing the boundary spacetimes¹ AdS_4 , $AdS_3 \times S^1$, $AdS_2 \times S^2$, $S^1 \times S^3$, and S^4 . We may write the AdS_5 metric for these various slicings as

$$ds^2 = d\rho^2 + \cosh^2 \rho ds_{AdS_{4-l}}^2 + \sinh^2 \rho d\Omega_l^2 \quad (2.3)$$

with $d\Omega_l^2$ the metric of the unit l -sphere S^l and $l = 0, \dots, 4$. When $l \leq 2$, the slicing includes $ds_{AdS_{4-l}}^2$, which denotes the AdS_{4-l} metric. We adopt a form for the AdS_{4-l} metric that is identical to Eq. (2.1), except for the replacement of the S^3 metric, $d\Omega_3^2$, by an S^{2-l} metric, $d\Omega_{2-l}^2$. When $l = 3$, we adopt a convention that $AdS_1 \equiv S^1$. Notice that the S^l collapses to zero volume at the center of AdS .

Not all of these boundary spacetimes have finite volume, but all introduce a spatial curvature scale into the dual SYM theory, allowing the otherwise scale-free $\mathcal{N} = 4$ SYM theory to undergo a thermal transition. We denote the Ricci scalar of the boundary spacetime as \mathcal{R} . For example, in $S^1 \times S^3$ slicing, $\mathcal{R} = 6/R_3^2$.

The supergravity theory is formulated on the ten-dimensional spacetime $AdS_5 \times S^5$ (or AdS_5 -Schwarzschild times S^5). Convenient forms of the S^5 metric that we will use are

$$d\Omega_5^2 = d\theta^2 + \sin^2 \theta d\Omega_{4-j}^2 + \cos^2 \theta d\Omega_j^2, \quad (2.4)$$

where j is any integer from 1 to 4, and θ runs from 0 to $\pi/2$.

2.2 Probe Dp-branes

We now introduce N_f flavor fields in the SYM theory, in the $N_f \ll N_c$ limit, which, in the supergravity description, corresponds to introducing Dp-branes probing the above geometries. Let us momentarily consider a background that is Poincaré-patch AdS_5 times S^5 , corresponding to the $\mathcal{N} = 4$ SYM theory in flat space and at zero temperature. This geometry arises as the near-horizon limit of a number $N_c \rightarrow \infty$ D3-branes [1].

Known supersymmetric embeddings of probe Dp-branes in this background include D7-branes extended along $AdS_5 \times S^3$ [6], D5-branes extended along $AdS_4 \times S^2$ [16–18], and D3-branes extended along $AdS_3 \times S^1$ [22]. Introducing D7-branes corresponds in the SYM theory to introducing $\mathcal{N} = 2$ supersymmetric hypermultiplets that transform in the fundamental representation of the gauge group and that propagate in 3+1 dimensions. Introducing D5-branes corresponds to introducing flavor fields that again transform in the fundamental representation of the gauge group, but that are confined to propagate along a (2+1)-dimensional defect. Similarly, introducing D3-branes corresponds to introducing flavor fields confined to propagate along a (1+1)-dimensional defect. More generally, any probe Dp-brane that is not extended along all of the AdS_5 directions will be dual to flavor fields confined to propagate along some defect. In each case, the flavor fields may be given a supersymmetry-preserving mass m . In the supergravity description, this mass m is encoded in the geometry of the Dp-brane in a way that we will make explicit below.

¹The choice of defining function can also determine the topology of the boundary. For example, a defining function with a zero at some point on the boundary may encode a collapsing cycle in the boundary spacetime.

In what follows, most of our attention will be focused on Dp -branes that are supersymmetric in Poincaré-patch AdS_5 times S^5 . In particular, we will present numerical results for D7-branes and D5-branes. We would like our analysis to be as general as possible, however, so we will not restrict the p value of the probe Dp -branes we study.

To introduce the Dp -brane's induced metric and action, we begin in the low-temperature phase, where the background geometry is global thermal $AdS_5 \times S^5$ (Eqs. (2.1) and (2.4)). The Dp -branes that we will study will be extended along $AdS_i \times S^j$, for some i and j that sum to $p + 1$. In other words, the Dp -brane will be extended along an AdS_i subspace inside global AdS_5 . This AdS_i subspace includes the radial and time directions as well as an S^{i-2} inside the S^3 of AdS_5 . The Dp -brane will also be extended along an S^j inside the S^5 factor. In the low-temperature phase, we will use the other slicings of global thermal AdS_5 , Eq. (2.3), only when studying D7-branes, which are extended in all of the AdS_5 directions ($i = 5$ and $j = 3$).

The Dp -brane may move in directions orthogonal to its worldvolume. We will allow the Dp -brane to move in the θ direction defined in Eq. (2.4) and, to preserve translation invariance in the dual field theory, we will allow θ to vary only as a function of the radial coordinate ρ . In other words, we allow the position of the $S^j \subset S^5$ to vary as the Dp -brane extends in the radial direction. From the Dp -brane worldvolume perspective, $\theta(\rho)$ is a scalar field. As we will review in detail below, this worldvolume scalar is dual to a SYM theory operator that is the (supersymmetric completion of) the mass operator of the flavor fields. This is how the mass m is encoded in the geometry of the Dp -brane. The induced Dp -brane worldvolume metric is

$$ds_{Dp}^2 = [1 + \theta'(\rho)^2] d\rho^2 + \cosh^2 \rho d\tau^2 + \sinh^2 \rho d\Omega_{i-2}^2 + \cos^2 \theta(\rho) d\Omega_j^2 \quad (2.5)$$

where the prime denotes differentiation with respect to ρ . In the high-temperature phase, the embeddings have the same form: AdS_i -Schwarzschild times $S^j \subset S^5$, and now the worldvolume scalar $\theta(z)$ depends only on z .

To determine $\theta(\rho)$, we need an equation of motion and boundary conditions. The equation of motion comes from the probe Dp -brane action, the Dirac-Born-Infeld (DBI) action,²

$$S_{Dp} = N_f T_{Dp} \int d^{(p+1)}\zeta \sqrt{\det(g_{ab})}, \quad (2.6)$$

where $T_{Dp} = (2\pi)^{-p} g_s^{-1} \alpha'^{-(p+1)/2}$ is the Dp -brane tension, ζ^a are worldvolume coordinates and g_{ab} is the induced metric on the Dp -brane, Eq. (2.5). The Dp -brane metric depends only on ρ (or z) and hence $\sqrt{\det(g_{ab})}$ will depend only on ρ (or z), so we will rescale the Dp -brane

²The full Dp -brane action of course describes the dynamics of a $U(1)$ worldvolume gauge field and all the worldvolume scalars (including $\theta(\rho)$, but also any others), and includes Wess-Zumino terms that describe the coupling of the Dp -brane fields to background fields, namely Ramond-Ramond form fields and the Neveu-Schwarz B-field. The equations of motion allow us to set to zero all components of the worldvolume field strength, as well as any other worldvolume scalars (besides our $\theta(\rho)$), in which case we may safely ignore the Wess-Zumino couplings and work with the action in Eq. (2.6).

action and work with an action density. Among the coordinates ζ^a , one will be the radial direction. Another will be the time direction. Integration over this direction simply produces a factor of $1/T$. The Dp -brane additionally has the internal directions of the $S^j \subset S^5$. Integration over these directions will produce the volume of a unit-radius j -sphere, V_j . For example, the D7-brane has $V_3 = 2\pi^2$. The remaining directions are spatial directions inside AdS_i . In $S^1 \times S^3$ slicing, these are the directions of the $S^{i-2} \subset S^3$. Integration over these directions then produces a factor of V_{i-2} . In the various other slicings, these directions are not all compact, so integration over these directions will not always yield a finite volume. We will divide both sides of Eq. (2.6) by the factor of $1/T$ and the integral over the spatial directions inside AdS_i , and define an action density

$$\tilde{S}_{Dp} \equiv \mathcal{N}_{Dp} \int d\rho \sqrt{\det(g_{ab})}. \quad (2.7)$$

where $\mathcal{N}_{Dp} \equiv N_f T_{Dp} V_j$. From now on, we will refer to \tilde{S}_{Dp} as the Dp -brane action.

To explain the boundary conditions on the worldvolume scalar, we begin in the high-temperature phase, where the background geometry is global AdS_5 -Schwarzschild times S^5 . We begin here because the story is essentially the same as for Dp -branes in Poincaré-patch AdS_5 -Schwarzschild times S^5 . In the high-temperature phase, two classes of Dp -brane embedding are possible. In the first class, which we will call “Minkowski” embeddings, the $S^j \subset S^5$ that the Dp -brane wraps is, at the boundary of AdS_5 -Schwarzschild, the maximum-volume equatorial S^j . As the Dp -brane extends into AdS_5 -Schwarzschild, the volume of the S^j shrinks (as described by $\theta(z)$) and, indeed, may shrink to zero volume at some radius outside the horizon, $z = \bar{z} < z_H$. The Dp -brane does not extend past \bar{z} , rather, it appears to end at \bar{z} [6] and does not intersect the AdS_5 -Schwarzschild horizon. Explicitly, the boundary conditions on $\theta(z)$ are that $\theta(\bar{z}) = \frac{\pi}{2}$, and $\theta'(\bar{z}) = \infty$ in order to avoid a conical singularity [13]. In the second class of embeddings, which we will call “black hole” embeddings, the $S^j \subset S^5$ shrinks as one moves into the bulk of AdS_5 -Schwarzschild but never collapses to zero volume, so the Dp -brane intersects the horizon, thus developing a worldvolume horizon. Explicitly, we have $\theta(z_H) \in [0, \frac{\pi}{2})$, and $\theta'(z_H) = 0$ in order for the embedding to be static. These two classes of embedding are distinguished by topology: in Minkowski embeddings the S^j collapses to zero volume, while in black hole embeddings only the thermal circle collapses to zero volume, at the horizon. The “critical solution” has $\bar{z} = z_H$, that is, the critical Dp -brane ends precisely at the horizon, and *both* the S^j and the thermal circle collapse to zero volume.

As first explained in Ref. [13], analogous embeddings exist in the low-temperature phase, but now the center of thermal AdS plays the role of the horizon. Minkowski embeddings now become “branes ending away from the center,” that is, the $S^j \subset S^5$ collapses to zero volume for some nonzero $\bar{\rho}$, with boundary conditions $\theta(\bar{\rho}) = \frac{\pi}{2}$ and $\theta'(\bar{\rho}) = \infty$. Black hole embeddings become “branes that reach the center,” that is, the $S^j \subset S^5$ never collapses to zero volume, and the Dp -brane extends all the way to $\rho = 0$, with boundary conditions $\theta(0) \in [0, \frac{\pi}{2})$ and $\theta'(0) = 0$. These two classes of embeddings are again distinguished by topology: for branes ending away from the center, the $S^j \subset S^5$ collapses to zero volume,



Figure 1: The two topologically distinct Dp -brane embeddings in thermal AdS . The vertical circle represents the S^j factor inside the S^5 , which can shrink to zero size in the left configuration, the horizontal circle represents the S^{i-2} factor inside of AdS_i , which can shrink to zero size in the right configuration.

while for branes that reach the center, the $S^{i-2} \subset AdS_i$ collapses to zero volume. These embeddings are depicted schematically in figure 1. The critical solution is now a Dp -brane that ends precisely at the center, so $\theta(0) = \frac{\pi}{2}$ and *both* the S^j and S^{i-2} collapse to zero volume at $\rho = 0$.

We will now explain in detail how the mass m of the flavor fields in the SYM theory, and the thermal expectation value of (the supersymmetric completion of) their mass operator, may be extracted from the Dp -brane geometry. To be concrete, consider the low-temperature phase. Inserting the worldvolume metric Eq. (2.5) into the action Eq. (2.7), we find

$$\tilde{S}_{Dp} = \mathcal{N}_{Dp} \int d\rho \cosh \rho (\sinh \rho)^{i-2} (\cos \theta)^j \sqrt{1 + \theta'^2}. \quad (2.8)$$

If we expand this action in a Taylor series in $\theta(\rho)$, we may identify, from the $\theta(\rho)^2$ term, a mass-squared for the worldvolume scalar, $M_\theta^2 = -j$ (in units of the AdS radius). Probe Dp -branes fall into two classes depending on whether or not M_θ^2 saturates the Breitenlohner-Freedman bound [23], $M^2 \geq -\frac{1}{4}(i-1)^2$, for a field in AdS_i with mass-squared M^2 . The field $\theta(\rho)$ for probe D5-branes and D7-branes *does not* saturate the Breitenlohner-Freedman bound, while $\theta(\rho)$ for probe D3-branes *does* saturate the Breitenlohner-Freedman bound.

One may relate M_θ^2 to the dimension Δ of the SYM theory operator dual to $\theta(\rho)$ in the usual fashion, $M_\theta^2 = [\Delta - (i-1)]\Delta$. What is the dual operator? The operator dual to $\theta(\rho)$ is given by the variation with respect to m of the SYM theory Lagrangian. We will denote this operator as \mathcal{O}_m . For example, consider the probe D7-brane. The dual field theory in this case is $\mathcal{N} = 4$ SYM theory coupled to $\mathcal{N} = 2$ supersymmetric hypermultiplets in the fundamental representation of the gauge group. The operator \mathcal{O}_m is the sum of three terms: the mass operator for the hypermultiplet fermions, m times the mass operator of the hypermultiplet scalars, and a term coupling these scalars to an adjoint scalar. The exact operator is written in Ref. [24]. The subscript on \mathcal{O}_m is a reminder that this operator depends explicitly on m . For our purposes thinking of \mathcal{O}_m as the mass operator of flavor fermions will be sufficient (we will not need the explicit form).

The DBI action, Eq. (2.8), yields the equation of motion for $\theta(\rho)$. Given a solution, we can extract the value of m from the asymptotic behavior of $\theta(\rho)$ [2,3]. The asymptotic behavior is most easily studied (in both the low- and high-temperature phases) using Fefferman-Graham

coordinates,

$$\theta(z) = z^{i-1-\Delta} \left\{ \theta_{(0)} + z \theta_{(1)} + \cdots + z^{2\Delta-i+1} [\theta_{(2\Delta-i+1)} + \psi_{(2\Delta-i+1)} \log z] + \cdots \right\}. \quad (2.9)$$

For Dp -branes that *do not* saturate the Breitenlohner-Freedman bound, the leading term, with coefficient $\theta_{(0)}$, is non-normalizable, while the sub-leading term with coefficient $\theta_{(2\Delta-i+1)}$ is normalizable. The equation of motion for $\theta(z)$ determines all other coefficients in terms of these two. These two coefficients will be fixed by the boundary conditions explained above, which thus completely specify the asymptotic behavior. In particular, for these cases the coefficient $\theta_{(0)}$ is related to the mass of the fundamental-representation fields as $m = \theta_{(0)}/(2\pi\alpha')$, or equivalently $\theta_{(0)} = 2\pi\sqrt{\lambda}m$. Notice that $\theta_{(0)}$ is dimensionless and that the right-hand side of this equation is written in units of the AdS radius. From the SYM theory perspective, in $S^1 \times S^3$ slicing, the more natural scale is the radius of the 3-sphere, R_3 . In our units, $R_3 = 1/2$, so we may write $\theta_{(0)} = 4\pi m R_3 / \sqrt{\lambda}$.

For Dp -branes that *do* saturate the Breitenlohner-Freedman bound, which have $2\Delta = i-1$, the coefficients $\theta_{(0)}$ and $\theta_{(2\Delta-i+1)}$ are identical. The leading logarithmic term, with coefficient $\psi_{(2\Delta-i+1)} = \psi_{(0)}$, is now non-normalizable, while the term with coefficient $\theta_{(0)}$ is normalizable. In the general analysis of section 3, we will use the notation appropriate for Dp -branes that *do not* saturate the Breitenlohner-Freedman bound, namely $\theta_{(0)}$ as the coefficient of the non-normalizable term and $\theta_{(2\Delta-i+1)}$ as the coefficient of the normalizable term. Converting to Dp -branes that *do* saturate the Breitenlohner-Freedman bound is easy: simply replace $\theta_{(0)} \rightarrow \psi_{(0)}$ and $\theta_{(2\Delta-i+1)} \rightarrow \theta_{(0)}$.

Following Ref. [25], we can extract the thermal expectation value $\langle \mathcal{O}_m \rangle$ from the asymptotic coefficients using holographic renormalization. Let F denote the contribution that the flavor fields make to the free energy density. $\langle \mathcal{O}_m \rangle$ is given by $\frac{\delta F}{\delta m}$. Using the AdS/CFT correspondence, F is given by the value of the on-shell DBI action Eq. (2.7), so we need to take the variation of the on-shell DBI action with respect to the leading, non-normalizable asymptotic value of $\theta(z)$. The problem that arises in doing this is that the radial integration will diverge at the boundary, $z = 0$. In holographic renormalization, we introduce a regulator by cutting off the integration at some small value, *i.e.*, we integrate only to $z = \epsilon$. We then introduce counterterms on the $z = \epsilon$ hypersurface to cancel divergences before removing the regulator by sending $\epsilon \rightarrow 0$. These counterterms are written in terms of $\theta(\epsilon)$ and the induced metric on the $z = \epsilon$ hypersurface, whose determinant we denote as γ . We denote the regulated action, plus counterterms, as \tilde{S}_{reg} , so that $\tilde{S}_{reg} = F$. We then have, for Dp -branes that *do not* saturate the Breitenlohner-Freedman bound [25, 26],

$$\langle \mathcal{O}_m \rangle = \lim_{\epsilon \rightarrow 0} \left(\frac{\epsilon^{-\Delta}}{\sqrt{\gamma}} \frac{\delta \tilde{S}_{reg}}{\delta \theta(\epsilon)} \right). \quad (2.10)$$

For Dp -branes that *do* saturate the Breitenlohner-Freedman bound, we must make the replacement $\epsilon^{-\Delta} \rightarrow \epsilon^{-\Delta} \log \epsilon$ [25]. The counterterms and explicit formulae for $\langle \mathcal{O}_m \rangle$ for the D7-brane, D5-brane and D3-brane are given in Refs. [13, 25].

Let us illustrate the procedure with an example: the probe D7-brane, which is extended along $AdS_5 \times S^3$ and so has $i = 5$, $j = 3$ and $M_\theta^2 = -j = -3$. The D7-brane thus *does not* saturate the Breitenlohner-Freedman bound for AdS_5 , $M^2 \geq -4$. The dual operator \mathcal{O}_m has dimension $\Delta = 3$. $\theta(z)$ has an asymptotic expansion

$$\theta(z) = \theta_{(0)} z + \theta_{(2)} z^3 + \psi_{(2)} z^3 \log z + \dots, \quad (2.11)$$

where $\psi_{(2)}$ is fixed in terms of $\theta_{(0)}$ as $\psi_{(2)} = \frac{1}{12} \mathcal{R} \theta_{(0)}$. The regulated action is $\tilde{S}_{reg} = \tilde{S}_{D7} + \sum_k \tilde{L}_k$, where the counterterms are [13, 25]

$$\tilde{L}_1 = -\frac{1}{4} \sqrt{\gamma}, \quad \tilde{L}_2 = \frac{1}{48} \sqrt{\gamma} \mathcal{R}_\gamma, \quad \tilde{L}_3 = -\frac{1}{32} (\log \epsilon) \sqrt{\gamma} \left(\mathcal{R}_{ij}^\gamma \mathcal{R}_\gamma^{ij} - \frac{1}{3} \mathcal{R}_\gamma^2 \right), \quad (2.12a)$$

$$\tilde{L}_4 = \frac{1}{2} \sqrt{\gamma} \theta(\epsilon)^2, \quad \tilde{L}_5 = -\frac{5}{12} \sqrt{\gamma} \theta(\epsilon)^4, \quad \tilde{L}_6 = \frac{1}{12} \log \theta(\epsilon) \sqrt{\gamma} \mathcal{R}_\gamma \theta(\epsilon)^2. \quad (2.12b)$$

where for clarity we have suppressed a factor of $\mathcal{N}_{D7} = N_f T_{D7} V_3 = \frac{1}{(2\pi)^4} \lambda N_f N_c$ that appears in every counterterm. Here \mathcal{R}_{ij}^γ and \mathcal{R}_γ are the Ricci tensor and Ricci scalar, respectively, of the induced metric on the $z = \epsilon$ hypersurface. Using Eq. (2.10), we find that the thermal expectation value of \mathcal{O}_m is given by

$$\langle \mathcal{O}_m \rangle = \mathcal{N}_{D7} \left[-2\theta_{(2)} + \frac{1}{3} \theta_{(0)}^3 + \frac{1}{6} \mathcal{R} \theta_{(0)} \log \theta_{(0)} \right]. \quad (2.13)$$

We will also present numerical results for a probe D5-brane, which is extended along $AdS_4 \times S^2$ and so has $i = 4$ and $j = 2$. The D5-brane has $M_\theta^2 = -j = -2$ and hence *does not* saturate the Breitenlohner-Freedman bound for AdS_4 , $M^2 \geq -\frac{9}{4}$. The dual operator \mathcal{O}_m has dimension $\Delta = 2$. In this case, the coefficient of the sub-leading, normalizable term is $\theta_{(2\Delta-i+1)} = \theta_{(1)}$. We will not present the counterterms explicitly. The result for the thermal expectation value of \mathcal{O}_m is $\langle \mathcal{O}_m \rangle = -\mathcal{N}_{D5} \theta_{(1)}$ [25], where $\mathcal{N}_{D5} = N_f T_{D5} V_2 = \frac{1}{2\pi^3} \sqrt{\lambda} N_f N_c$.

3. Scaling Analysis

In this section we perform a scaling analysis similar to that of Refs. [11, 14, 27] for probe Dp-branes in global thermal AdS , probe Dp-branes in global AdS -Schwarzschild, and probe D7-branes in the various other slicings of global thermal AdS . We find the relevant scaling exponents for probe Dp-brane embeddings and determine when those exponents are real or complex. We also confirm via numerical analysis that complex exponents signal a first order transition in the dual SYM theory.

3.1 Probe Dp-branes in $S^1 \times S^3$ Slicing: Low-temperature Phase

We begin with probe Dp-branes in global thermal AdS , corresponding to the SYM theory in the low-temperature, confined phase. We first note that the flavor physics, within the low temperature phase of the SYM theory, is completely independent of temperature. The global thermal AdS metric Eq. (2.1) does not depend on the temperature T , which thus appears in the DBI action Eq. (2.6) only via an overall factor from integration over the thermal S^1

(which is then hidden in the rescaled action Eq. (2.7)). Consequently, the equation of motion for $\theta(\rho)$, and its boundary conditions, are T -independent. As a result, the expectation value $\langle \mathcal{O}_m \rangle$ in the dual SYM theory will be independent of T . This temperature independence is not unexpected — it is a property of the leading large- N_c behavior of generic observables (not involving Wilson loops which wrap the thermal circle) in the low temperature phase of non-Abelian gauge theories [28–30]. Our supergravity analysis is thus valid for any temperature below the Hawking-Page transition temperature, $T < T_{HP} = \frac{3}{2\pi}$. The remaining relevant scales in the SYM theory are the hypermultiplet mass m and the radius R_3 of the 3-sphere. The physics we are interested in will depend only on these scales, or more accurately on their dimensionless product mR_3 .

We now turn to the scaling analysis. We focus on the region near the center of AdS , and expand the metric to leading nontrivial order using $\sinh \rho \approx \rho$, $\cosh \rho \approx 1$. We first consider the critical solution, that is, fluctuations of the form $\theta(\rho) = \pi/2 + \delta\theta(\rho)$ with $\delta\theta(\rho)$ small. We may then use $\cos \theta \approx -\delta\theta$. The critical solution has the boundary condition $\delta\theta(0) = 0$. The Dp -brane action, Eq. (2.8), becomes

$$\tilde{S}_{Dp} = \mathcal{N}_{Dp} \int d\rho \rho^{i-2} \delta\theta^j \sqrt{1 + \delta\theta'^2}, \quad (3.1)$$

with, once again, $i + j = p + 1$. The resulting equation of motion for $\delta\theta(\rho)$ is

$$\rho \delta\theta \delta\theta'' + [(i-2)\delta\theta \delta\theta' - j\rho] (1 + \delta\theta'^2) = 0. \quad (3.2)$$

This equation has an important scaling symmetry under which

$$\delta\theta(\rho) \rightarrow \mu \delta\theta(\rho) \quad \text{and} \quad \rho \rightarrow \mu\rho, \quad (3.3)$$

for real, positive μ . In other words, a single solution $\delta\theta(\rho) = f(\rho)$ gives rise to a one-parameter family of solutions $\delta\theta(\rho) = \mu^{-1}f(\mu\rho)$. The solution of Eq. (3.2) for the critical embedding, which we denote $\delta\theta^*(\rho)$, is

$$\delta\theta^*(\rho) \equiv \rho \sqrt{\frac{j}{i-2}}. \quad (3.4)$$

Notice that $\delta\theta^*(\rho)$ is invariant under the scaling transformation.

Next, we seek solutions near the critical one, still in the near-center region, of the form

$$\delta\theta(\rho) = \delta\theta^*(\rho) + \xi(\rho). \quad (3.5)$$

The fluctuation $\xi(\rho)$ has the linearized equation of motion

$$\rho^2 \xi'' + a\rho \xi' + a\xi = 0, \quad (3.6)$$

with $a = j + (i - 2)$. This has solutions $\xi(\rho) = \pm\rho^{\beta_{\pm}}$ with

$$\beta_{\pm} = \frac{1}{2} \left[(1 - a) \pm \sqrt{a^2 - 6a + 1} \right]. \quad (3.7)$$

The β_{\pm} are the scaling exponents. Depending on the value of a , the scaling exponents β_{\pm} may be real or complex. Physically, $a = j + (i - 2)$ is the dimension of the sub-manifold of the Dp -brane worldvolume that collapses to zero volume in the critical solution: the j dimensions of the $S^j \subset S^5$ and the $i - 2$ dimensions of the $S^{i-2} \subset AdS_i$. For the present case of probe Dp -branes in $S^1 \times S^3$ slicing, the dimension a of the collapsing submanifold is simply $p - 1$, but this will not be the case in subsequent examples.

Explicit values of the exponents, for various choices of a , appear in Table 1. As shown in the table, the critical value of a is 6: for $a < 6$ the near-center, near-critical solutions have complex exponents, while for $a \geq 6$ they have real exponents.

The perturbed solution,

$$\delta\theta(\rho) = \delta\theta^*(\rho) + \alpha_+ \rho^{\beta_+} + \alpha_- \rho^{\beta_-}, \quad (3.8)$$

must obey the scaling symmetry. This implies that the coefficients α_{\pm} must scale as

$$\alpha_{\pm} \rightarrow \mu^{1-\beta_{\pm}} \alpha_{\pm}. \quad (3.9)$$

The coefficients α_{\pm} are determined by the boundary conditions, specifically, the value of $\bar{\rho}$ or $\theta(0)$. This is why α_{\pm} are “charged” under the scaling transformation: because $\bar{\rho}$ and $\theta(0)$ are not invariant under scaling.

A solution that is near the critical solution in the near-center region will remain so all the way out to the asymptotic region.³ The boundary condition deep inside AdS_i (the value of $\bar{\rho}$ or $\theta(0)$) must fix both the asymptotic coefficients $\theta_{(0)}$ and $\theta_{(2\Delta-i+1)}$ and the near-center coefficients α_{\pm} . The asymptotic coefficients can thus be thought of as functions of the near-center coefficients. Sufficiently close to the critical solution, the α_{\pm} will be very small and hence the asymptotic coefficients may be linearly related to the near-center coefficients. Put more simply, we may Taylor expand $\theta_{(0)}$ and $\theta_{(2\Delta-i+1)}$ to linear order in α_{\pm} . Let $\theta_{(0)}^*$ and $\theta_{(2\Delta-i+1)}^*$ denote the asymptotic coefficients of the critical solution. We then have, for a near-critical solution,

$$\theta_{(0)} - \theta_{(0)}^* = A_{(0)}^+ \alpha_+ + A_{(0)}^- \alpha_-, \quad (3.10a)$$

$$\theta_{(2\Delta-i+1)} - \theta_{(2\Delta-i+1)}^* = A_{(2\Delta-i+1)}^+ \alpha_+ + A_{(2\Delta-i+1)}^- \alpha_-, \quad (3.10b)$$

for some set of coefficients A^{\pm} . Notice that the overall sign of $\xi(\rho)$ is arbitrary, so the form of Eq. (3.10) is valid for both $\theta_{(0)} < \theta_{(0)}^*$ and $\theta_{(0)} > \theta_{(0)}^*$, that is, for Dp -branes that end at the center and for Dp -branes that end away from the center. We may now ask what the scaling transformation of the α_{\pm} , Eq. (3.9), teaches us about the asymptotic coefficients, and what we may then conclude in the SYM theory about the behavior of $\langle \mathcal{O}_m \rangle$ as a function of m .

³More formally, we expect the critical solution to be an attractor solution as one moves toward the AdS boundary. In Ref. [27], this was shown explicitly for Dp -branes in Poincaré-patch AdS -Schwarzschild.

a	β_{\pm}
7	$-3 \pm \sqrt{2}$
6	$-\frac{5}{2} \pm \frac{1}{2}$
5	$-2 \pm i$
4	$-\frac{3}{2} \pm i\frac{\sqrt{7}}{2}$
3	$-1 \pm i\sqrt{2}$
2	$-\frac{1}{2} \pm i\frac{\sqrt{7}}{2}$

Table 1: Scaling exponents β_{\pm} for probe Dp -branes whose critical solution has a collapsing submanifold of dimension a .

For complex β_{\pm} , if we perform the scaling transformation Eq. (3.9) we find that, as functions of μ , $(\theta_{(0)} - \theta_{(0)}^*)$ and $(\theta_{(2\Delta-i+1)} - \theta_{(2\Delta-i+1)}^*)$ will acquire terms of the form $\mu^{1-\text{Re}\beta_{\pm}}$ times either a sine or cosine of $\text{Im}\beta_{\pm} \log \mu$. Notice that $1 - \text{Re}\beta_{\pm} > 0$ in all cases. Consequently, sending $\mu \rightarrow 0$ produces solutions which, in the $(\theta_{(0)}, \theta_{(2\Delta-i+1)})$ plane, spiral inward toward a limit point which corresponds to the critical solution. More precisely, the arbitrary overall sign of $\xi(\rho)$ leads to two intertwined spirals, as illustrated below in Fig. 3(b).

In the dual field theory, we may argue, following Refs. [11, 14], that $\langle \mathcal{O}_m \rangle$ must jump discontinuously from the outer branch of one spiral to the outer branch of the other as the mass m is varied. Such discontinuous behavior signals a first-order phase transition. We then expect discontinuous behavior in generic observables associated with the flavor fields, of which $\langle \mathcal{O}_m \rangle$ is simply the most convenient to compute from the supergravity perspective.

To be concrete, let us analyze the example of probe D5-branes extended along $AdS_4 \times S^2$, for which $a = 4$ and $\beta_{\pm} = -\frac{3}{2} \pm i\frac{\sqrt{7}}{2}$. Recall that in this case $m = \theta_{(0)}/(2\pi\alpha')$, and $\langle \mathcal{O}_m \rangle = -\mathcal{N}_{D5}\theta_{(1)}$ where the operator \mathcal{O}_m has dimension $\Delta = 2$ and $\mathcal{N}_{D5} = \frac{1}{2\pi^3}\lambda^{1/2}N_fN_c$. Figure 2 shows the value of $\tilde{S}_{reg}/\mathcal{N}_{D5}$ for the D5-brane as a function of $\theta_{(0)}$, and figure 3 shows the numerical result for solutions in the $(\theta_{(0)}, \theta_{(1)})$ plane.

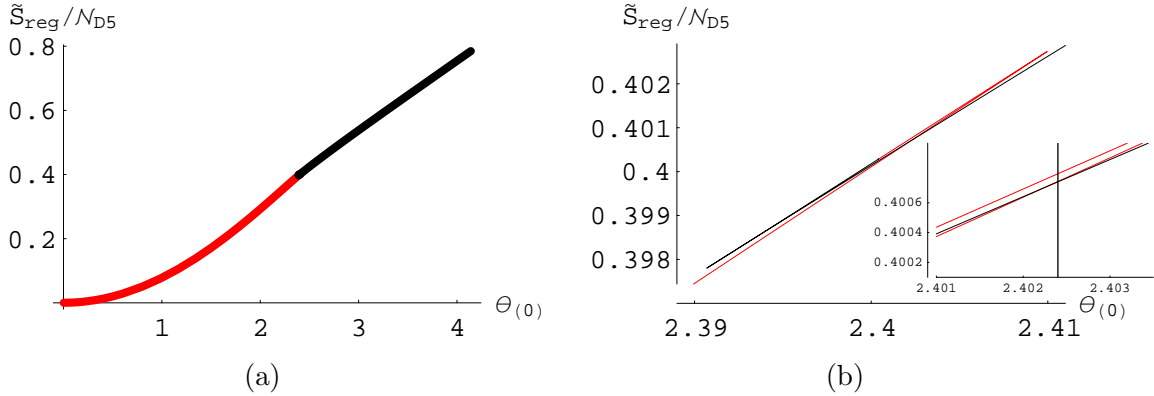


Figure 2: (a.) $\tilde{S}_{reg}/\mathcal{N}_{D5}$ as a function of $\theta_{(0)}$ for the D5-brane probe in global thermal AdS in $S^1 \times S^3$ slicing. The red curves correspond to D5-branes that reach the center of AdS while the black curves correspond to D5-branes that end away from the center. The point at which the red and black curves meet corresponds to the critical solution. (b.) Close-up of (a.) near the critical solution. The inset figure shows a further close-up. The vertical line in the inset figure indicates where the transition occurs, at the critical value $\theta_{(0)}^{crit} \approx 2.402$.

In these and all subsequent plots for global thermal AdS , the red curves arise from Dp -brane solutions that reach the center of AdS , while the black curves arise from Dp -branes ending away from the center. For global AdS_5 -Schwarzschild, red curves arise from Dp -branes that reach the horizon while black curves arise from Dp -branes that end outside the horizon. The critical solution will thus always be where the red and black curves meet.

In figure 2, we see that the free energy, which is always the minimal value of the regulated action \tilde{S}_{reg} , has a small kink (a discontinuous first derivative) as a function of $\theta_{(0)}$. Since

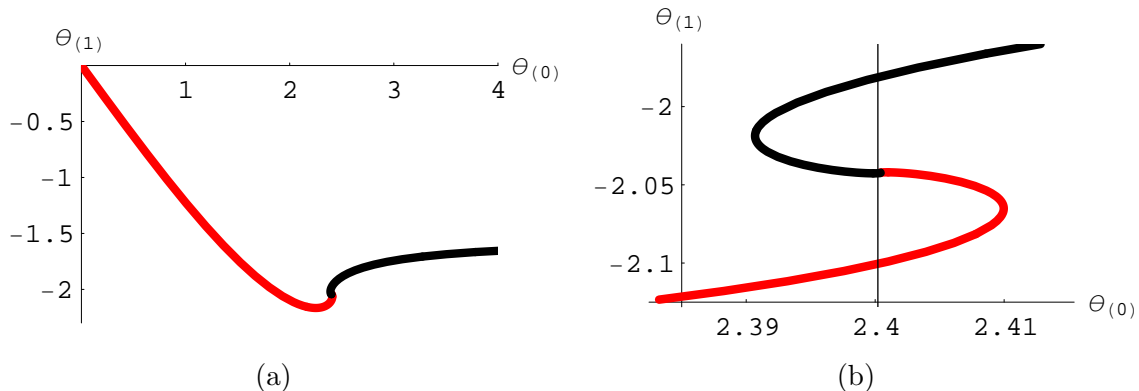


Figure 3: (a.) $\theta_{(1)}$ as a function of $\theta_{(0)}$ for the D5-brane probe in global thermal AdS in $S^1 \times S^3$ slicing. The red curves correspond to D5-branes that reach the center of AdS while the black curves correspond to D5-branes that end away from the center. The point at which the red and black curves meet corresponds to the critical solution. (b.) Close-up of (a.) near the critical solution. The vertical line indicates where the transition occurs, at the critical value $\theta_{(0)}^{crit} \approx 2.400$. As we increase $\theta_{(0)}$, moving along the red curve from left to the right, the physical value of $\theta_{(1)} = -\langle \mathcal{O}_m \rangle / \mathcal{N}_{D5}$ jumps upward at $\theta_{(0)}^{crit}$, from the red curve to the top-most arm of the black curve.

$m = \theta_{(0)} / (2\pi\alpha')$, we conclude that a first-order phase transition occurs in the SYM theory as a function of the mass m . (The free energy is always continuous, but at a first order transition its first derivative jumps.) The transition occurs at the critical value⁴ $\theta_{(0)}^{crit} = 4\pi m R_3 / \sqrt{\lambda} = 2.400$ or equivalently $m = \sqrt{\lambda} \theta_{(0)}^{crit} / (4\pi R_3) = 0.191 \sqrt{\lambda} / R_3$. Using $\langle \mathcal{O}_m \rangle = \frac{\delta F}{\delta m} = -\mathcal{N}_{D5} \theta_{(1)}$, we see precisely this behavior in figure 3, as $\theta_{(1)}$ jumps discontinuously from one arm of the spiral to the other. When the embedding equations have multiple solutions for a given value of $\theta_{(0)}$, only those solutions that minimize the free energy (\tilde{S}_{reg}) represent genuine equilibrium states. These minimal free-energy solutions only lie on the outermost branches of the two spiral arms. As shown in Refs. [14, 19], moving inward along the red or black curves toward the critical solution, a new tachyon appears in the meson spectrum at every turn of the spiral, providing a clear signal of instability. Notice also that $m^* \sim 1/R_3$, as expected from the fact that generic observables will be T -independent in the low-temperature phase, as mentioned above. Clearly this transition is a finite-volume effect.

When the scaling exponents β_{\pm} are real, the story is very different. Now the scaling transformation of Eq. (3.9) is a simple rescaling, and no spiral will appear in the $(\theta_{(0)}, \theta_{(2\Delta-i+1)})$ plane. The most interesting example is the probe D7-brane,⁵ extended along $AdS_5 \times S^3$,

⁴Notice that the result for $\theta_{(0)}^{crit}$ as computed from the free energy in figure 2 is $\theta_{(0)}^{crit} \approx 2.402$, which is slightly larger than the value $\theta_{(0)}^{crit} \approx 2.400$ obtained from figure 3, where we used an equal-area method. We attribute the difference to numerical error in estimating the location of the “kink” in figure 2. Here, and for all subsequent branes, the location of the transition that we will use is that computed from the equal-area method.

⁵We have also formally analyzed a D8-brane extended along $AdS_5 \times S^4$, which has $a = 7$, and found behavior similar to that for the D7-brane. A D8-brane carries no conserved charge in type IIB supergravity,

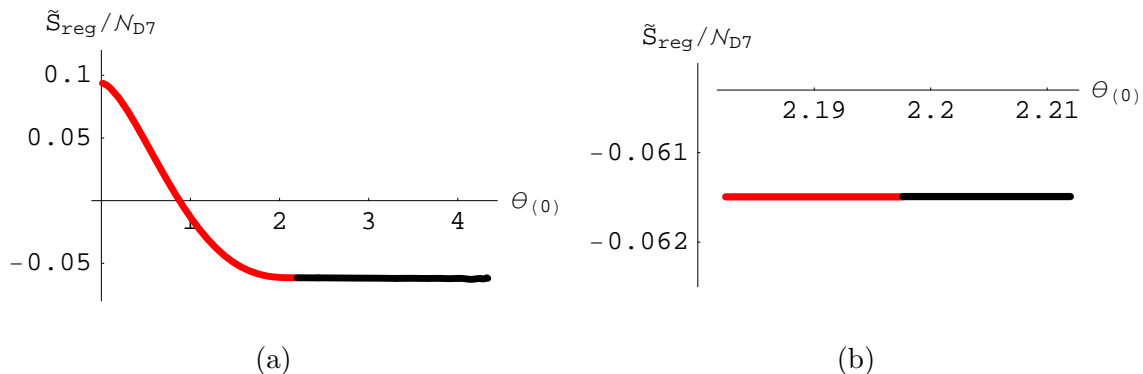


Figure 4: (a.) $\tilde{S}_{reg}/\mathcal{N}_{D7}$ as a function of $\theta_{(0)}$ for the D7-brane probe in global thermal AdS in $S^1 \times S^3$ slicing. (b.) Close-up of (a.) near the critical solution. The critical solution (where the red and black curves meet) has $\theta_{(0)}^* \approx 2.198$.

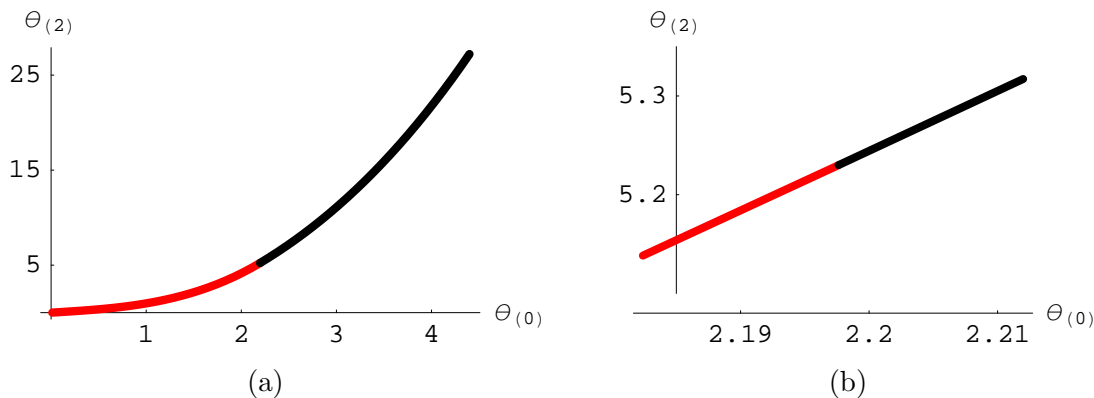


Figure 5: (a.) $\theta_{(2)}$ as a function of $\theta_{(0)}$ for the D7-brane probe in global thermal AdS in $S^1 \times S^3$ slicing. (b.) Close-up of (a.) near the critical solution. The critical solution (where the red and black curves meet) has $\theta_{(0)}^* \approx 2.198$ and $\theta_{(2)}^* \approx 5.230$.

for which $a = 6$ and $\beta_{\pm} = -\frac{5}{2} \pm \frac{1}{2} = \{-2, -3\}$. Recall that in this case $m = \theta_{(0)}/(2\pi\alpha')$ and $\langle \mathcal{O}_m \rangle$ is given by Eq. (2.13) where the operator \mathcal{O}_m has dimension $\Delta = 3$. Recall also that $\mathcal{N}_{D7} = \frac{1}{(2\pi)^4} \lambda N_f N_c$. Figure 4 shows $\tilde{S}_{reg}/\mathcal{N}_{D7}$ as a function of $\theta_{(0)}$ for the D7-brane, which has a continuous first derivative. Figure 5 shows $\theta_{(2)}$ as a function of $\theta_{(0)}$, which is single-valued. The critical solution has $\theta_{(0)}^* \approx 2.198$ and $\theta_{(2)}^* \approx 5.230$. In terms of SYM theory quantities, the critical solution has $m^* = \sqrt{\lambda} \theta_{(0)}^*/(4\pi R_3) = 0.1748\sqrt{\lambda}/R_3$. (Notice again that $m^* \sim 1/R_3$.) We conclude that no first-order transition occurs in the SYM theory. We expect some kind of non-analyticity in the SYM theory, however, because in the supergravity description the topology of the D7-brane changes in passing through the critical solution. In section 4 we will show that certain observables have divergent behavior at the critical point, and we will examine how this transition affects the meson spectrum.

however, and is therefore unstable.

3.2 Probe Dp -branes in $S^1 \times S^3$ Slicing: High-temperature Phase

We will now perform the scaling analysis for probe Dp -branes in global AdS_5 -Schwarzschild, corresponding to the SYM theory in the high-temperature, deconfined phase. Our result will be essentially the same as that of Refs. [11, 14]: all probe Dp -branes have complex exponents β_{\pm} and hence exhibit a spiral in the $(\theta_{(0)}, \theta_{(2\Delta-i+1)})$ plane, implying that first-order transitions appear in the respective SYM theories. For the D7-brane, this must be the case in order to agree with the numerical results in $S^1 \times S^3$ slicing [13] and in Poincaré patch AdS_5 -Schwarzschild [7–9, 11–14], which we interpret as the high- T limit of the theory formulated on global AdS_5 -Schwarzschild, as explained in section 2.1.

The critical solution is now a Dp -brane that ends precisely at the horizon. At the horizon only the thermal S^1 inside AdS_i -Schwarzschild collapses to zero volume. This is the key difference from thermal AdS_i . For the critical solution, the $S^j \subset S^5$ will still collapse, but now *all* probe Dp -brane critical embeddings will have the same collapsing S^1 . The S^{i-2} that collapsed in thermal AdS_i are replaced with this S^1 in AdS_i -Schwarzschild, so we expect $a = j + 1$. We can thus jump to the answer: as the largest value of j that allows for $\theta(z)$ is $j = 4$, none of the Dp -brane probes can have $a > 6$, and hence all must have complex β_{\pm} .

To confirm this, we proceed in the same spirit as above. We now focus on the near-horizon region. Let $z = z_H + Z$ and $\theta(z) = \frac{\pi}{2} + \delta\theta(Z)$. We expand the metric coefficients to leading nontrivial order. The induced Dp -brane metric is then

$$ds_{Dp}^2 = (1 + \delta\theta'^2) dZ^2 + \frac{2}{z_H^2} \frac{Z^2}{1 - z_H^2} d\tau^2 + \mathcal{F}(z_H) d\Omega_{i-2}^2 + \delta\theta^2 d\Omega_j^2. \quad (3.11)$$

The Dp -brane action, ignoring overall Z -independent constants that do not affect $\delta\theta$'s equation of motion, is

$$S_{Dp} \propto \int dZ Z \delta\theta^j \sqrt{1 + \delta\theta'^2}. \quad (3.12)$$

This is of precisely the same form as Eq. (3.1) but with $i-2 \rightarrow 1$ so indeed $a = j+1$ and all Dp -brane probes will have complex exponents β_{\pm} and exhibit a spiral in the $(\theta_{(0)}, \theta_{(2\Delta-i+1)})$ plane. The action Eq. (3.12) is in fact identical to the near-horizon action written in Refs. [11, 14] for Dp -brane probes in the Rindler space that arises as the near-horizon geometry of Poincaré patch AdS -Schwarzschild.

3.3 Probe D7-brane in Other Slicings: Low-Temperature Phase

By using different slicings, leading to different boundary geometries, we can change the dimension of the critical solution's collapsing submanifold, as different slicings lead to spheres of different dimension, $S^l \subset AdS_5$ for $l = 0, \dots, 4$, that collapse to zero volume at the center of AdS_5 (see Eq. (2.3)). We will focus on the D7-brane and the low-temperature phase because lower-dimensional Dp -branes, or Dp -branes in the high-temperature phase, will not be able to reach $a \geq 6$. For the D7-brane, the dual SYM theory is $\mathcal{N} = 4$ SYM theory coupled to massive $\mathcal{N} = 2$ hypermultiplets, formulated on different four-manifolds, in the low-temperature, confining phase.

Using the $AdS_{4-l} \times S^l$ slicing of AdS_5 , the induced D7-brane metric is

$$ds_{D7}^2 = [1 + \theta'(\rho)^2] d\rho^2 + \cosh^2 \rho ds_{AdS_{4-l}}^2 + \sinh^2 \rho d\Omega_l^2 + \cos^2 \theta(\rho) d\Omega_3^2, \quad (3.13)$$

and the D7-brane action is

$$\tilde{S}_{D7} = \mathcal{N}_{D7} \int d\rho (\cosh \rho)^{4-l} (\sinh \rho)^l (\cos \theta)^3 \sqrt{1 + \theta'^2}. \quad (3.14)$$

In the near-center limit this becomes

$$\tilde{S}_{D7} = \mathcal{N}_{D7} \int d\rho \rho^l \delta\theta^3 \sqrt{1 + \delta\theta'^2} \quad (3.15)$$

which is the same as Eq. (3.1), but with $i - 2 \rightarrow l$ and $j = 3$, so $a = l + 3$ and we will have complex exponents β_{\pm} for $l = 0, 1, 2$ and real exponents β_{\pm} for $l = 3, 4$.

As an example of complex exponents, consider the $l = 2$ case, $AdS_2 \times S^2$ slicing, with $a = 5$ and complex exponents $\beta_{\pm} = -2 \pm i$. We expect a spiral in the $(\theta_{(0)}, \theta_{(2)})$ plane. Figure 6 shows the numerical result for $\theta_{(2)}$ as a function of $\theta_{(0)}$, which indeed exhibits a spiral, so we again have a first-order transition. In this case, the transition occurs at the critical value $\theta_{(0)}^{crit} = m/(2\pi\alpha') = 1.6557$ or equivalently $m = \sqrt{\lambda} \theta_{(0)}^{crit}/(2\pi) = 0.2635 \sqrt{\lambda}$ times the inverse of the AdS curvature radius.

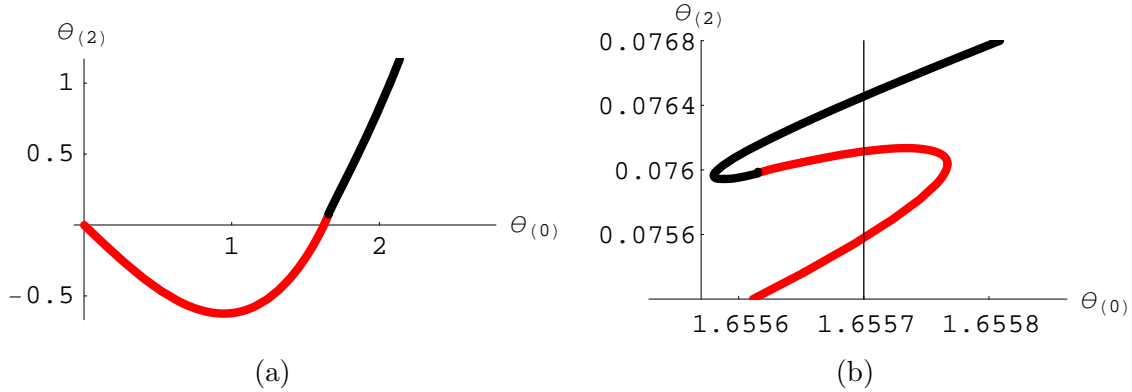


Figure 6: (a.) $\theta_{(2)}$ as a function of $\theta_{(0)}$ for the D7-brane in $AdS_2 \times S^2$ -sliced thermal AdS_5 . (b.) Close-up of (a.) near the critical solution. The vertical line indicates where the transition occurs, at the critical value $\theta_{(0)}^{crit} \approx 1.6557$.

We have two examples of real exponents. The first example is the $l = 3$ case, $S^1 \times S^3$ slicing, which was examined above (see figures 4 and 5) and will be examined in detail in the next section. The second example is the $l = 4$ case, S^4 slicing, with $a = 7$, giving real exponents, $\beta_{\pm} = -3 \pm \sqrt{2}$. We expect $\theta_{(2)}$ to be single-valued as a function of $\theta_{(0)}$. Figure 7 shows the numerical result for $\theta_{(2)}$ as a function of $\theta_{(0)}$, which is indeed single-valued. We have verified numerically that the solutions exhibit scaling behavior with the exponents $\beta_{\pm} = -3 \pm \sqrt{2}$. In this case the critical solution has $\theta_{(0)}^* \approx 2.6395$ and $\theta_{(2)}^* \approx 14.5943$. In terms of SYM theory quantities the critical solution has $m^* = \sqrt{\lambda} \theta_{(0)}^*/(2\pi) \approx 0.42\sqrt{\lambda}$ times the inverse of the AdS curvature radius.

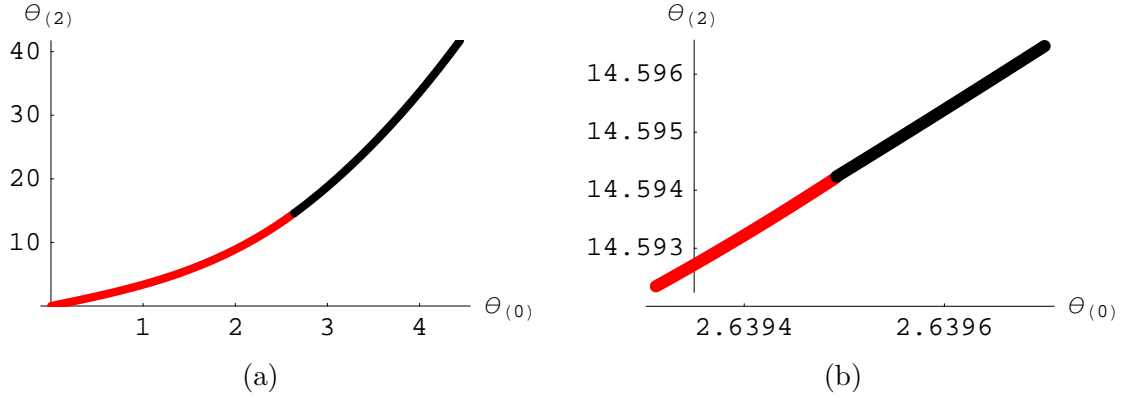


Figure 7: (a.) $\theta_{(2)}$ as a function of $\theta_{(0)}$ for the D7-brane in S^4 -sliced thermal AdS . (b.) Close-up of (a.) near the critical solution. The critical solution (where the red and black curves meet) has $\theta_{(0)}^* \approx 2.6395$ and $\theta_{(2)}^* \approx 14.5943$.

4. Characterizing the Transition

Let us summarize our story so far. Whether a Dp -brane probe exhibits a spiral in the $(\theta_{(0)}, \theta_{(2\Delta-i+1)})$ plane or not depends upon the value of a , the dimension of the submanifold of the critical embedding that collapses to zero volume. When $a < 6$, a spiral does appear and, as discussed above, we may conclude that the dual SYM theory has a first order phase transition associated with the flavor fields.

To study what happens when $a \geq 6$, we will restrict our attention to the D7-brane in $S^1 \times S^3$ slicing. The D7-brane undergoes a topology change, but $\theta_{(2)}$ is single-valued as a function of $\theta_{(0)}$ (or mass). In the SYM theory, we expect a transition to occur, but evidently it is not first order.

In this section, we will exhibit divergences at the critical point in several observables in the dual SYM theory, and examine the associated critical exponents. We will also show that the transition manifests itself in the meson spectrum as a cusp in the spectrum of a particular scalar meson. We will also argue that the transition will be “smoothed out” for any large but finite value of λ , or in other words that the transition is an artifact of the $\lambda \rightarrow \infty$ limit.

4.1 The Behavior of $\langle \mathcal{O}_m \rangle$

We want to know what the scaling transformation Eq. (3.9) implies for the observable $\langle \mathcal{O}_m \rangle$. Returning to Eq. (3.10), we perform the scaling transformation in Eq. (3.9), using $1 - \beta_+ = 3$ and $1 - \beta_- = 4$, with the result

$$\theta_{(0)} - \theta_{(0)}^* = A_{(0)}^+ \alpha_+ \mu^3 + A_{(0)}^- \alpha_- \mu^4, \quad (4.1a)$$

$$\theta_{(2)} - \theta_{(2)}^* = A_{(2)}^+ \alpha_+ \mu^3 + A_{(2)}^- \alpha_- \mu^4. \quad (4.1b)$$

Notice again that, as in Eq. (3.10), the form of these equations (and the equations below that follow from them) is the same for both $\theta_{(0)} > \theta_{(0)}^*$ and $\theta_{(0)} < \theta_{(0)}^*$. Using the first equation

to eliminate μ gives, to leading order in the deviation from criticality, $\mu \sim (\theta_{(0)} - \theta_{(0)}^*)^{1/3}$. Plugging this into the second equation will generate a non-analytic $(\theta_{(0)} - \theta_{(0)}^*)^{4/3}$ term as well as an analytic $(\theta_{(0)} - \theta_{(0)}^*)$ piece. Translating to field theory quantities using $\theta_{(0)} \propto m$ and Eq. (2.13), we find that $\langle \mathcal{O}_m \rangle$ contains non-analytic terms of the form

$$\langle \mathcal{O}_m \rangle \sim (m - m^*)^{4/3} + \dots, \quad (4.2)$$

in addition to contributions analytic in m near m^* . Here \dots is an expansion in higher powers of $(m - m^*)^{1/3}$. The key point is that $\langle \mathcal{O}_m \rangle$ has a divergent second derivative with respect to m at m^* . The expectation $\langle \mathcal{O}_m \rangle$ is the derivative of the free energy F with respect to m , and hence the *third* derivative of the free energy diverges as $m \rightarrow m^*$,

$$\frac{\partial^3}{\partial m^3} F \sim (m - m^*)^{-2/3}, \quad (4.3)$$

from which we identify a critical exponent of $2/3$.

4.2 Static Test Charges

Consider, in the dual SYM theory, the interaction between static fundamental-representation test charges. Focus, for simplicity, on the case of an infinitely heavy quark and antiquark which are maximally separated — sitting at opposite poles of the S^3 . The change in free energy due to inserting the static quark and antiquark is given by ($-T$ times) the logarithm of the expectation value of the Polyakov loop (or Wilson line) correlator, with the two Polyakov loops sitting at antipodal poles in space.

Roughly speaking, in the dual gravitational description (in the $N_c \rightarrow \infty$ and $\lambda \rightarrow \infty$ limits), this Polyakov loop correlator is given by the regularized minimal area of a string worldsheet with an $S^1 \times S^1$ boundary, where the S^1 's wrap the thermal circle and are maximally separated in the boundary spacetime. More precisely, the objects that have simple supergravity descriptions are the supersymmetric extensions of Wilson loops (“Maldacena loops”). These correspond to adding a line integral of a linear combination of the SYM scalars to the exponent of the Polyakov loop [31]. Exactly what linear combination is determined by choosing, arbitrarily, some six-dimensional unit vector, or equivalently some point in S^5 . In the dual description, the boundary of the string worldsheet must be located at the chosen point in the S^5 factor of the boundary geometry.

We will focus, for simplicity, on the maximally symmetric case where the Maldacena loops are located at a pole of the S^5 , or in other words are maximally separated (in the boundary geometry) from the D7-brane wrapping an S^3 equator of the S^5 . This choice preserves the full $SO(4)$ R -symmetry of the SYM theory with fundamental hypermultiplets. The antipodal locations of the loops means that the correlator is also invariant under an $SO(3)$ subgroup of the $SO(4)$ spatial rotation symmetry group, as well as $U(1)$ time translations.

Given this setup, an extremal string worldsheet, preserving all the symmetries of the correlator, will be one that stretches across global AdS_5 while everywhere sitting at the pole of the S^5 . This is illustrated in figure 8 (B.).

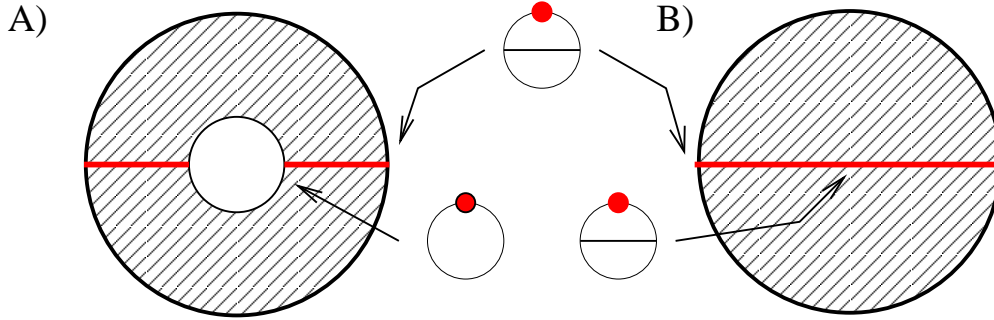


Figure 8: (A.) The disk depicts global AdS_5 in $S^1 \times S^3$ slicing. The perimeter represents the boundary while the center represents the center of AdS_5 . The shaded/striped area represents a D7-brane that ends before reaching the center. The red lines represent two segments of a string, each stretching from the boundary to the D7-brane’s endpoint. Each of the three circles between (A.) and (B.) represents the S^5 . The D7-brane, wrapping an $S^3 \subset S^5$, is depicted as a black line. The location of the string(s) is depicted by a red dot. At the boundary, the D7-brane wraps the equatorial S^3 , but at its endpoint it reaches the pole of the S^5 , where the strings also sits (of the circles between (A.) and (B.), compare the top one and the lower left one). (B.) The same picture as in (A.), but now the D7-brane does not end at finite radial coordinate, rather it extends all the way to the center. Indeed, the figure depicts the trivial embedding, in which the D7-brane wraps the equatorial S^3 everywhere. Notice that in this case the string and D7-brane never coincide on the S^5 .

If the D7-brane embedding fills the the whole AdS_5 space and reaches the center, then the wrapped $S^3 \subset S^5$ never collapses to zero volume (so $0 < \theta(\rho = 0) < \frac{\pi}{2}$), and the D7-brane never intersects the string worldsheet. This is not the case for D7-brane embeddings that end outside the center (at some $\rho = \bar{\rho}$ where $\theta(\bar{\rho}) = \frac{\pi}{2}$). Such D7-branes reach the pole of the internal S^5 and intersect the string worldsheet at $\bar{\rho}$. This allows the string to break, so that its worldsheet ends on the D7-brane instead of extending all the way to the center of global AdS . This is illustrated in figure 8 (A.). Phrased differently, for Minkowski embeddings of the D7-brane, a maximal-symmetry string worldsheet with an $(S_1)^4$ boundary exists — with two of the S^1 ’s on the AdS boundary and the other two on the D7-brane at a point of closest approach to the global AdS center. Again, the two possibilities are depicted in figure 8.

The potential energy of the static quark and antiquark is directly proportional to the length of the string. The difference in length of the strings in the two configurations is just the diameter of the “hole” in the center of the D7-brane configuration. For the near-critical embeddings, this is directly proportional to the scaling parameter μ . Therefore the difference in the static quark-antiquark potential energy (for this maximally-symmetric configuration) between near-critical and critical values of the quark mass will be proportional to $\mu \sim (m - m^*)^{1/3}$ (or $(m^* - m)^{1/3}$ for $m < m^*$)— and thus non-analytic in the quark mass at m^* .

The behavior of this Polyakov loop correlator has an intuitive explanation in terms of screening lengths. To understand this, first consider the physics of QCD (in flat space) at low temperature, where two infinitely massive test quarks will have a flux tube, or QCD string, stretching between them. The energy E in this QCD string is its tension, σ , times its length,

L : $E = \sigma L$. The theory also has dynamical quarks, however, which can cause sufficiently long flux tubes to break. If the test quarks are pulled sufficiently far apart, then the energy in the string will exceed the point at which the creation of a dynamical quark-antiquark pair is energetically favorable. In other words, when $E > 2m$ for a dynamical quark mass m , the string can snap and the single heavy-heavy meson will decay into two heavy-light mesons. Define a “screening length” as the length L_s at which the pair production occurs and the QCD string snaps. Equating $\sigma L_s = 2m$, we see that the screening length is *proportional* to the mass of the quark, $L_s \propto m$.

Now consider the $\mathcal{N} = 4$ SYM theory formulated on \mathbb{R}^3 coupled to massive $\mathcal{N} = 2$ hypermultiplets. The story is a bit different since the theory is conformal. This implies that the static quark potential is Coulombic, and vanishes at large separation. Naïvely, one might think that this would imply that pair production of dynamical massive quarks would never be energetically favorable. (After all, hydrogen is not unstable to electron/positron pair creation!) This argument relies on our *weak*-coupling intuition, however. If the coupling is sufficiently strong, then the light-heavy binding energy can become comparable to the light quark mass m . In this regime a heavy-heavy meson, pulled apart to large separation, can indeed decay to a pair of light-heavy mesons via pair production of a light quark-antiquark pair. This scenario is sometimes called Gribov confinement [32]. For the $\mathcal{N} = 4$ SYM theory, this process was analyzed in detail in Ref. [33]. The screening length, beyond which the system will pair produce dynamical quarks, must by scale invariance be proportional to the inverse of the light quark mass, $L_s \propto 1/m$.

Finally, consider the $\mathcal{N} = 4$ SYM theory formulated on S^3 with $\mathcal{N} = 2$ matter. As we lower the dynamical quark mass we find that at some point this screening length becomes larger than the diameter of the sphere, $L_s > 2R_3$. Beyond this point, a (maximally separated) static quark-antiquark pair is stable against pair production of dynamical quarks. Our Polyakov loop correlator exhibits precisely this behavior.

4.3 The Meson Spectrum

In the $\mathcal{N} = 4$ SYM theory coupled to $\mathcal{N} = 2$ matter on $S^1 \times \mathbb{R}^3$, the first-order phase transition of the fundamental-representation fields is characterized by “meson melting.” At low temperature the meson spectrum is gapped and discrete while at high temperature it becomes gapless and continuous [11, 14, 34]. A natural question for the theory on S^3 , then, is what happens to the meson spectrum at the transition we have found?

For conceptual simplicity, and for technical reasons that will become clear shortly, in this section only we will take the temperature T to be precisely zero. We are allowed to do so because, as explained above, the D7-brane physics we are interested in is independent of temperature in the low-temperature phase. We are thus free to take $T = 0$ and study the SYM theory formulated on the four-manifold $\mathbb{R} \times S^3$ with \mathbb{R} the (Minkowski-signature, non-compact) time direction.

At zero temperature we have a simple intuitive picture of what happens. Consider first the infinite-volume case at finite temperature. If the mass m is fixed and we heat the system

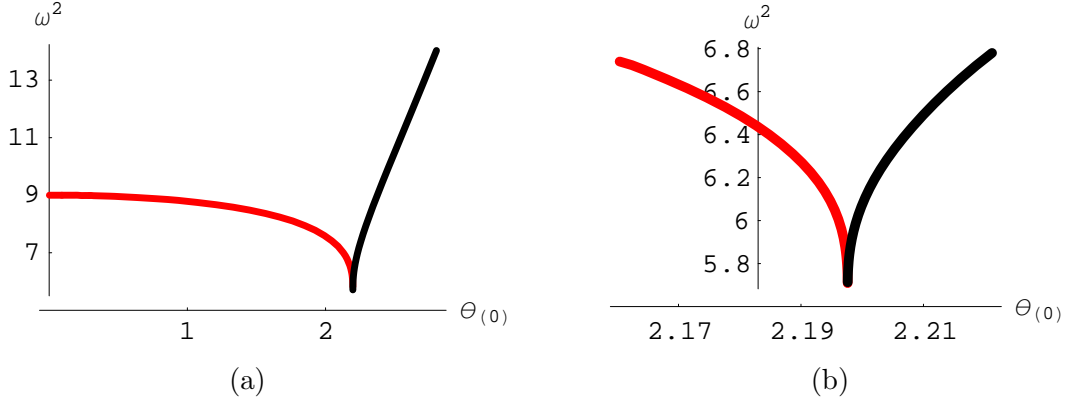


Figure 9: (a.) Scalar meson frequency squared (times the AdS radius squared) versus $\theta_{(0)}$. The critical solution has $\theta_{(0)}^* = 2.198$ and $(\omega^*)^2 = 5.7$. (b.) Close-up of (a.) near the critical solution. Our analytic arguments (confirmed numerically in figure 10) show that the curves behave as $(\theta_{(0)} - \theta_{(0)}^*)^{1/3}$ near the critical solution.

up, stable bound mesons fall apart at the “melting” temperature. What we are instead doing here may be viewed as fixing the mass and then squeezing the system, at zero temperature, into smaller and smaller volume and asking what happens to mesonic bound states as R_3 passes through the critical radius $R_3^* = 0.1748\sqrt{\lambda}/m$. We expect the mesons to fall apart as their zero point energy due to confinement within the finite volume becomes larger than their binding energy.

Before discussing the meson spectrum in detail, we should define precisely what we mean by a meson mass. On $\mathbb{R} \times S^3$, a state is classified by its $SO(4)$ angular momentum $l(l+2)$, for non-negative integer l , and its energy eigenvalue ω , governing the behavior under time translations. We will use this energy eigenvalue ω to characterize a meson state, and will refer to ω as the meson mass.⁶ We will only consider states that are in an $l=0$ s -wave on S^3 , and compute the dependence of ω^2 on the quark mass m , or more precisely (but equivalently) on $\theta_{(0)}$. States with higher l are expected to have higher energy. As explained in Ref. [35], the meson spectrum can be computed in the supergravity description by expanding the DBI action to quadratic order in fluctuations and then solving the resulting linearized equations of motion. The fluctuations may be those of either the embedding geometry or of the D7-brane worldvolume gauge fields.

We first study a fluctuation of the D7-brane geometry of the form

$$\theta(\rho) \rightarrow \theta(\rho, t) = \theta_B(\rho) + \phi(\rho)e^{i\omega t}, \quad (4.4)$$

⁶In some literature on holographic mesons in flat space, the name “meson mass” is used for the magnitude of an imaginary spatial wave vector \vec{k} for which an eigenstate of the supergravity small fluctuation operator exists. These eigenvalues characterize the leading long distance fall-off of equilibrium Euclidean space correlators in the dual field theory. On S^3 , no (interesting) analogue of this definition exists. The spatial (angular) momentum simply takes values $l(l+2)$ for non-negative integers l ; since the space is finite we have no notion of the asymptotic behavior of correlation functions.

where $\theta_B(\rho)$ is a static background solution, as computed in section 3.1. This fluctuation will be dual to a scalar meson in the SYM theory. To determine ω , we employ a shooting technique in which we fix the boundary condition for $\phi(\rho)$ at the *AdS* boundary and iteratively adjust ω until the physical boundary condition at the D7-brane endpoint (or the center) is satisfied. At the *AdS* boundary, we demand that the fluctuation be normalizable and hence must scale, in Fefferman-Graham coordinates, as $O(\epsilon^3)$ with the cutoff $z = \epsilon$. For D7-branes that reach the center, we then demand that the fluctuation must have vanishing first derivative at the center. For D7-branes ending away from the center, we require that the $S^3 \subset S^5$ collapse without a conical deficit, as explained in section 2.2. Translating the results into field theory quantities, the resulting spectrum of ω^2 versus $\theta_{(0)} = 4\pi\sqrt{\lambda}mR_3$ for this scalar meson is shown in figure 9. We see a pronounced kink precisely at the critical solution, $\theta_{(0)} = \theta_{(0)}^*$. The kink does not extend down to $\omega^2 = 0$; the minimal value is $\omega^2 \approx 5.7$ times the square of the *AdS* radius, or equivalently $\omega^2 \approx 22.8R_3^2$.

Using scaling symmetry arguments, we can show analytically that this kink in the scalar meson spectrum has the precise form $\omega - \omega^* \sim (m - m^*)^{1/3}$ as $m \rightarrow m^*$ (from above or below). We begin by solving analytically for the fluctuation in the near-center limit. At zero temperature the action for $\theta(\rho, t)$ is

$$\tilde{S}_{D7} = \mathcal{N}_{D7} \int d\rho dt (\cos \theta)^3 (\sinh \rho)^3 \sqrt{(1 + \theta'^2)(\cosh^2 \rho - \dot{\theta}^2) + \dot{\theta}^2 \theta'^2}. \quad (4.5)$$

We take the same near-center limit as in section 3.1, insert Eq. (4.4), and expand to quadratic order in the fluctuation $\phi(\rho)$ to find the linearized equation of motion. We choose the background solution to be the critical solution $\theta_B(\rho) = \theta^*(\rho) = \frac{\pi}{2} + \rho$, so the frequency of the fluctuation is the critical one, $\omega = \omega^*$. The resulting equation for $\phi(\rho)$,

$$\rho^2 \phi''(\rho) + 6\rho \phi'(\rho) + (6 + 2\omega^{*2}\rho^2) \phi(\rho) = 0, \quad (4.6)$$

has a solution

$$\begin{aligned} \phi(\rho) &= \frac{1}{\rho^3} \left[c_0^* \cos(\sqrt{2}\omega^*\rho) + c_1^* \frac{\sin(\sqrt{2}\omega^*\rho)}{\sqrt{2}\omega^*} \right] \\ &= c_0^* \rho^{-3} + c_1^* \rho^{-2} + O(\rho^{-1}), \end{aligned} \quad (4.7)$$

where c_0^* and c_1^* are integration constants. The background is the critical solution, for which the brane ends at the center, $\rho = 0$. Normalizability at $\rho = 0$ requires $c_0^* = 0$. We could then fix the value of ω^* by imposing normalizability at the *AdS* boundary as follows.

Normalizability at the boundary requires that $\phi(\rho)$'s contribution to the leading, non-normalizable asymptotic coefficient (which was $\theta_{(0)}$ in Fefferman-Graham coordinates) must vanish. We denote this contribution as

$$\Phi^*(c_1^*, \omega^*) = f_1(\omega^*) c_1^* + O(c_1^{*2}) = 0, \quad (4.8)$$

where, as indicated, this may be a function of c_1^* and ω^* and we have linearized in c_1^* , which is taken to be small. We could then solve the equation $f_1(\omega^*) = 0$ to find the value of ω^* .

We next want to find the shifted frequency, $\omega = \omega^* + \delta\omega$, of fluctuations of near-critical solutions. More precisely, we need to determine how $\delta\omega = \omega - \omega^*$ scales with $\mu \sim (m - m^*)^{1/3}$. Near-critical solutions will have nonzero values for c_0 and $c_1 = c_1^* + \delta c_1$ so that:

$$\begin{aligned}\theta(\rho, t) &= \rho + \alpha_- \rho^{-3} + \alpha_+ \rho^{-2} + \phi(\rho) e^{i\omega t} \\ &= \rho + (\alpha_- + c_0 e^{i\omega t}) \rho^{-3} + (\alpha_+ + c_1 e^{i\omega t}) \rho^{-2} + O(\rho^{-1}).\end{aligned}\tag{4.9}$$

We see that c_0 must scale the same way as α_- , and c_1 the same as α_+ , that is $c_0 \rightarrow \mu^4 c_0$ and $c_1 \rightarrow \mu^3 c_1$. To fix the value of ω , we again impose the condition of normalizability at the *AdS* boundary, which requires that the coefficient $\Phi(c_1, c_0, \omega)$ of the non-normalizable term vanish,

$$\begin{aligned}0 = \Phi(c_1, c_0, \omega) &= f_1(\omega) c_1 + f_2(\omega) c_0 \\ &= [f_1(\omega^*) + f_1'(\omega^*) \delta\omega] (c_1^* + \delta c_1) + [f_2(\omega^*) + f_2'(\omega^*) \delta\omega] c_0 \\ &= f_1'(\omega^*) \delta\omega c_1^* + f_2(\omega^*) c_0,\end{aligned}\tag{4.10}$$

where we have linearized everything treating δc_1 , c_0 and $\delta\omega$ as the same order of smallness and used $f_1(\omega^*) = 0$. We may immediately solve for $\delta\omega = \omega - \omega^*$ with the result

$$\omega - \omega^* = -\frac{f_2(\omega^*)}{f_1'(\omega^*)} \frac{c_0}{c_1^*}.\tag{4.11}$$

Notice $f_2(\omega^*)$ and $f_1'(\omega^*)$ do not transform under the scaling symmetry: they are just numbers. Since c_0 scales as μ^4 while c_1^* scales as μ^3 , the result of Eq. (4.11) shows that $\omega - \omega^* \sim \mu \sim (m - m^*)^{1/3}$. Notice that these arguments hold for both $m > m^*$ or $m < m^*$ (the results do not depend on whether the near-critical solution in Eq. (4.9) has $\theta_{(0)} > \theta_{(0)}^*$ or $\theta_{(0)} < \theta_{(0)}^*$). Figure 10 shows our numerical data for $\ln |\omega - \omega^*|$ versus $\ln |\theta_{(0)} - \theta_{(0)}^*|$ and a linear fit to the data, with good agreement between this asymptotic form and the numerical results.

This non-analytic behavior appears to manifest itself only for the geometric fluctuation of the embedding function $\theta(\rho)$. Solving for the other fluctuation in the geometry (the other S^5 direction orthogonal to the S^3) we can compute the spectrum for a second scalar meson. The result appears in figure 11. We see no kink at $\theta_{(0)}^*$. We also computed the meson spectra corresponding to fluctuations of the D7-brane's worldvolume gauge field as described in Ref. [35]. These meson spectra are similar to figure 11. In particular, they exhibit no kinks. We confirmed that all of our meson spectra reduce to the known results of Ref. [35] in the limits of either zero or large mass.

4.4 Light String States

In section 4.1, we showed that the third derivative of the free energy F diverges at m^* . In other words, some three-point coupling in an effective theory describing flavored mesons in this strongly-coupled SYM theory is diverging as m approaches m^* . One question this immediately raises is whether this power-law growth of the three-point coupling continues for

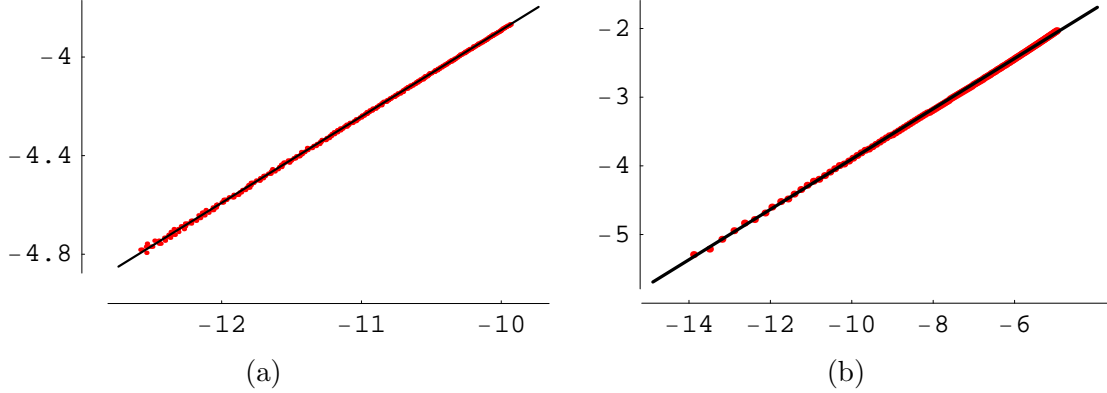


Figure 10: (a.) $\ln|\omega - \omega^*|$ (with ω in units of the inverse AdS radius) versus $\ln|\theta_{(0)} - \theta_{(0)}^*|$ for D7-branes that end at the center, which have $\theta_{(0)} < \theta_{(0)}^*$ (corresponding to the red curves in the previous figure). The solid black line is a numerical fit to a functional form $C_1 + C_2 \ln|\theta_{(0)} - \theta_{(0)}^*|$. Our analytic argument predicts $C_2 = 1/3$. The numerical result is $C_1 \approx -0.38$ and $C_2 \approx 0.35$. (b.) The same quantities as in (a.) but now for D7-branes that end away from the center, which have $\theta_{(0)} > \theta_{(0)}^*$ (the black curves in the previous figure). The solid black line is a numerical fit of the same form as in (a.) with the result $C_1 \approx -0.24$ and $C_2 \approx 0.36$.

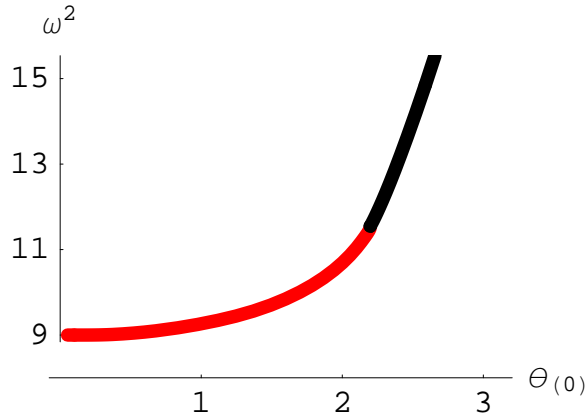


Figure 11: Scalar meson frequency squared (times the AdS radius squared) versus $\theta_{(0)}$ for the meson holographically dual to the second fluctuation of the D7-brane geometry. The punchline here is that no “kink” appears, in contrast to the spectrum in figure 9.

arbitrarily small values of $m - m^*$, and if so, what is the physical meaning of this singularity? We will argue that for any large, but *finite*, values of λ , the scaling regime will be cut off at small values of $m - m^*$, so the divergence in the three-point coupling is an artifact of the strict $\lambda \rightarrow \infty$ limit.

Our evidence comes from the string theory side of the correspondence: the scaling regime is cut off by stringy corrections. To see this, note that the scalar curvature of the D7-brane’s

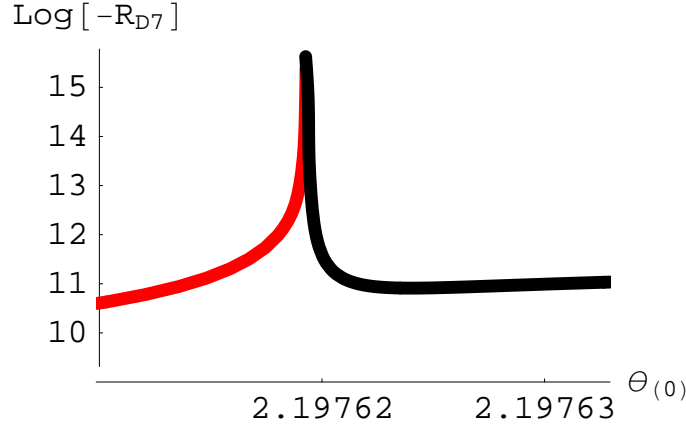


Figure 12: Log of minus the scalar curvature of the D7-brane, $\ln[-\mathcal{R}_{D7}]$ (in units of the AdS radius), evaluated at the point of closest approach to the center of AdS , versus asymptotic coefficient $\theta_{(0)}$ in $S^1 \times S^3$ slicing. The red curve represents D7-branes that reach the center, for which $\ln[-\mathcal{R}_{D7}]$ is evaluated at the center. The black curve represents D7-branes that end away from the center, for which $\ln[-\mathcal{R}_{D7}]$ is evaluated at the endpoint.

induced metric, \mathcal{R}_{D7} , in the near-center limit, is

$$\mathcal{R}_{D7} = -12 \frac{\delta\theta^2 \delta\theta'^2 - \frac{3}{2} \rho \delta\theta \delta\theta' + \rho^2}{\rho^2 \delta\theta^2 (1 + \delta\theta'^2)}. \quad (4.12)$$

For the critical embedding, $\delta\theta^*(\rho) = \rho$, the curvature diverges as ρ^{-2} near the endpoint $\rho = 0$. For near-critical solutions, the curvature is finite at the endpoint (or center), but grows without limit as one approaches the critical solution⁷. For branes that reach the center, $\delta\theta' = 0$ at the center and hence \mathcal{R}_{D7} scales as $\delta\theta^{-2}$. For solutions ending away from the center, $\delta\theta'$ diverges, and the curvature at the endpoint scales as ρ^{-2} . Under a scaling transformation, both ρ and $\delta\theta$ scale as μ , so the curvature in either case will scale as μ^{-2} .

When the scalar curvature of the induced metric becomes of order of the string scale, $\alpha'^{-1} \equiv \ell_s^{-2}$, stringy corrections to the DBI action will no longer be negligible, and hence our analysis of the scaling behavior (based entirely on the DBI action) will cease to be valid. In other words, higher order corrections will become important when $\mu^{-2} \sim \ell_s^{-2}$. These corrections are due to excited open string modes whose mass naïvely goes as ℓ_s^{-1} , but whose mass is reduced by a power of μ when the endpoints of the string are in the high-curvature region. To illustrate this issue graphically, we plot $\ln[-\mathcal{R}_{D7}]$ in figure 12, evaluated at the point of closest approach to the center, as a function of the asymptotic coefficient $\theta_{(0)}$.

Using $\alpha'^{-1} \equiv \ell_s^{-2} \sim \sqrt{\lambda}$ and $\mu \sim (\theta_{(0)} - \theta_{(0)}^*)^{1/3} = (m - m^*)^{1/3}$, the condition $\mu^{-2} \sim \ell_s^{-2}$ becomes $(m - m^*) \sim \lambda^{-3/4}$. The properties of the boundary theory are thus governed by the critical exponents we calculated above, but only in the range of masses $\lambda^{-3/4}/R_3 \ll$

⁷For the D7-brane in $S^1 \times \mathbb{R}^3$ slicing (with its first order transition), the scalar curvature also diverges for the critical solution, but in this case the critical solution lies on an unphysical (infinitely unstable) branch.

$(m - m^*) \ll 1/R_3$. (Once again, the same relations are true for $m < m^*$, with $m - m^*$ replaced by $m^* - m$, etc.) In particular, in this window the three-point function of the zero-momentum \mathcal{O}_m operator grows as $(m - m^*)^{-2/3}$. This power law growth will eventually be cut off at the lower end of the scaling window. As λ is a free parameter, however, we are free to consider the regime where this scaling window extends over arbitrarily many decades.

5. Conclusion

The scaling symmetry of near-center or near-horizon probe Dp -brane solutions in global AdS has allowed us to determine when phase transitions associated with fundamental-representation fields coupled to $\mathcal{N} = 4$ SYM theory will be first order or continuous. When they are continuous, we find that the approach to criticality is governed by non-trivial critical exponents which can be calculated analytically using the supergravity description. We emphasize that the phase transitions we have found are finite-volume, large- N_c , and large- λ effects. The continuous transition we find in the D7-brane case can be interpreted as a meson binding/unbinding transition similar to the finite-temperature case analyzed in previous studies.

A finite volume in the flavored SYM theory can give rise to interesting new effects in the phase diagram, such as the appearance of our continuous phase transition. We have only explored a small part of the multi-dimensional phase diagram of this theory. Probe Dp -brane techniques can be used to study systems at finite density [24, 36–39] or in background electric and magnetic fields [19, 20, 40–44]. We expect a rich phase structure to emerge for these systems when confined to finite volume.

Acknowledgments

This work was supported in part by the U.S. Department of Energy under Grant No. DE-FG02-96ER40956. The work of A.O’B. was also supported in part by the Jack Kent Cooke Foundation and by the Cluster of Excellence for Fundamental Physics “Origin and Structure of the Universe.” A. O’B. would like to thank the Perimeter Institute and the Aspen Center for Physics for hospitality during the completion of this work.

References

- [1] J. M. Maldacena, *The large N limit of superconformal field theories and supergravity*, *Adv. Theor. Math. Phys.* **2** (1998) 231–252, [[hep-th/9711200](#)].
- [2] E. Witten, *Anti-de Sitter space and holography*, *Adv. Theor. Math. Phys.* **2** (1998) 253–291, [[hep-th/9802150](#)].
- [3] S. S. Gubser, I. R. Klebanov, and A. M. Polyakov, *Gauge theory correlators from non-critical string theory*, *Phys. Lett.* **B428** (1998) 105–114, [[hep-th/9802109](#)].
- [4] E. Witten, *Anti-de Sitter space, thermal phase transition, and confinement in gauge theories*, *Adv. Theor. Math. Phys.* **2** (1998) 505–532, [[hep-th/9803131](#)].

- [5] S. S. Gubser, I. R. Klebanov, and A. W. Peet, *Entropy and temperature of black 3-branes*, *Phys. Rev.* **D54** (1996) 3915–3919, [[hep-th/9602135](#)].
- [6] A. Karch and E. Katz, *Adding flavor to AdS/CFT*, *JHEP* **06** (2002) 043, [[hep-th/0205236](#)].
- [7] J. Babington, J. Erdmenger, N. J. Evans, Z. Guralnik, and I. Kirsch, *Chiral symmetry breaking and pions in non-supersymmetric gauge / gravity duals*, *Phys. Rev.* **D69** (2004) 066007, [[hep-th/0306018](#)].
- [8] I. Kirsch, *Generalizations of the AdS/CFT correspondence*, *Fortsch. Phys.* **52** (2004) 727–826, [[hep-th/0406274](#)].
- [9] K. Ghoroku, T. Sakaguchi, N. Uekusa, and M. Yahiro, *Flavor quark at high temperature from a holographic model*, *Phys. Rev.* **D71** (2005) 106002, [[hep-th/0502088](#)].
- [10] R. Apreda, J. Erdmenger, N. Evans, and Z. Guralnik, *Strong coupling effective Higgs potential and a first order thermal phase transition from AdS/CFT duality*, *Phys. Rev.* **D71** (2005) 126002, [[hep-th/0504151](#)].
- [11] D. Mateos, R. C. Myers, and R. M. Thomson, *Holographic phase transitions with fundamental matter*, *Phys. Rev. Lett.* **97** (2006) 091601, [[hep-th/0605046](#)].
- [12] T. Albash, V. G. Filev, C. V. Johnson, and A. Kundu, *A topology-changing phase transition and the dynamics of flavour*, [hep-th/0605088](#).
- [13] A. Karch and A. O’Bannon, *Chiral transition of $N = 4$ super Yang-Mills with flavor on a 3-sphere*, *Phys. Rev.* **D74** (2006) 085033, [[hep-th/0605120](#)].
- [14] D. Mateos, R. C. Myers, and R. M. Thomson, *Thermodynamics of the brane*, *JHEP* **05** (2007) 067, [[hep-th/0701132](#)].
- [15] S. W. Hawking and D. N. Page, *Thermodynamics of black holes in anti-de Sitter space*, *Commun. Math. Phys.* **87** (1983) 577.
- [16] A. Karch and L. Randall, *Open and closed string interpretation of SUSY CFT’s on branes with boundaries*, *JHEP* **06** (2001) 063, [[hep-th/0105132](#)].
- [17] O. DeWolfe, D. Z. Freedman, and H. Ooguri, *Holography and defect conformal field theories*, *Phys. Rev.* **D66** (2002) 025009, [[hep-th/0111135](#)].
- [18] J. Erdmenger, Z. Guralnik, and I. Kirsch, *Four-Dimensional Superconformal Theories with Interacting Boundaries or Defects*, *Phys. Rev.* **D66** (2002) 025020, [[hep-th/0203020](#)].
- [19] V. G. Filev, *Criticality, scaling and chiral symmetry breaking in external magnetic field*, **0706.3811**.
- [20] V. G. Filev and C. V. Johnson, *Universality in the Large N_c Dynamics of Flavour: Thermal Vs. Quantum Induced Phase Transitions*, *JHEP* **10** (2008) 058, [[arXiv:0805.1950](#)].
- [21] C. Fefferman and C. Graham, *Conformal Invariants*, in ‘*The Mathematical Heritage of Elie Cartan*’, (*Asterisque*, 1985) 95, .
- [22] N. R. Constable, J. Erdmenger, Z. Guralnik, and I. Kirsch, *Intersecting D3-branes and holography*, *Phys. Rev.* **D68** (2003) 106007, [[hep-th/0211222](#)].
- [23] P. Breitenlohner and D. Z. Freedman, *Stability in gauged extended supergravity*, *Ann. Phys.* **144** (1982) 249.

- [24] S. Kobayashi, D. Mateos, S. Matsuura, R. C. Myers, and R. M. Thomson, *Holographic phase transitions at finite baryon density*, *JHEP* **02** (2007) 016, [[hep-th/0611099](#)].
- [25] A. Karch, A. O’Bannon, and K. Skenderis, *Holographic renormalization of probe D-branes in AdS/CFT*, *JHEP* **04** (2006) 015, [[hep-th/0512125](#)].
- [26] S. de Haro, S. N. Solodukhin, and K. Skenderis, *Holographic reconstruction of spacetime and renormalization in the AdS/CFT correspondence*, *Commun. Math. Phys.* **217** (2001) 595–622, [[hep-th/0002230](#)].
- [27] V. P. Frolov, *Merger transitions in brane-black-hole systems: Criticality, scaling, and self-similarity*, *Phys. Rev.* **D74** (2006) 044006, [[gr-qc/0604114](#)].
- [28] F. Neri and A. Gocksch, *Chiral symmetry restoration in large N QCD at finite temperature*, *Phys. Rev.* **D28** (1983) 3147.
- [29] R. D. Pisarski, *Finite temperature QCD at large N* , *Phys. Rev.* **D29** (1984) 1222.
- [30] P. Kovtun, M. Unsal, and L. G. Yaffe, *Volume independence in large N_c QCD-like gauge theories*, *JHEP* **06** (2007) 019, [[hep-th/0702021](#)].
- [31] J. M. Maldacena, *Wilson loops in large n field theories*, *Phys. Rev. Lett.* **80** (1998) 4859–4862, [[hep-th/9803002](#)].
- [32] V. N. Gribov, *Orsay lectures on confinement*, [hep-ph/9403218](#), [9404332](#), [9905285](#).
- [33] A. Karch, E. Katz, and N. Weiner, *Hadron masses and screening from AdS Wilson loops*, *Phys. Rev. Lett.* **90** (2003) 091601, [[hep-th/0211107](#)].
- [34] C. Hoyos, K. Landsteiner, and S. Montero, *Holographic meson melting*, *JHEP* **04** (2007) 031, [[hep-th/0612169](#)].
- [35] M. Kruczenski, D. Mateos, R. C. Myers, and D. J. Winters, *Meson spectroscopy in AdS/CFT with flavour*, *JHEP* **07** (2003) 049, [[hep-th/0304032](#)].
- [36] K. Ghoroku, M. Ishihara, and A. Nakamura, *$D3/D7$ holographic gauge theory and chemical potential*, [0708.3706](#).
- [37] A. Karch and A. O’Bannon, *Holographic thermodynamics at finite baryon density: Some exact results*, [0709.0570](#).
- [38] D. Mateos, S. Matsuura, R. C. Myers, and R. M. Thomson, *Holographic phase transitions at finite chemical potential*, [0709.1225](#).
- [39] T. Faulkner and H. Liu, *Condensed matter physics of a strongly coupled gauge theory with quarks: some novel features of the phase diagram*, [arXiv:0812.4278](#).
- [40] V. G. Filev, C. V. Johnson, R. C. Rashkov, and K. S. Viswanathan, *Flavoured large N gauge theory in an external magnetic field*, [hep-th/0701001](#).
- [41] T. Albash, V. Filev, C. V. Johnson, and A. Kundu, *Finite temperature large N gauge theory with quarks in an external magnetic field*, [0709.1547](#).
- [42] J. Erdmenger, R. Meyer, and J. P. Shock, *AdS/CFT with flavour in electric and magnetic Kalb-Ramond fields*, [0709.1551](#).

- [43] T. Albash, V. Filev, C. V. Johnson, and A. Kundu, *Quarks in an external electric field in finite temperature large N gauge theory*, 0709.1554.
- [44] V. G. Filev, C. V. Johnson, and J. P. Shock, *Universal Holographic Chiral Dynamics in an External Magnetic Field*, arXiv:0903.5345.